Convective Initiation near the Andes in Subtropical South America

K. L. RASMUSSEN

Mesoscale and Microscale Meteorology Laboratory, National Center for Atmospheric Research, Boulder, Colorado

R. A. HOUZE JR.

Department of Atmospheric Sciences, University of Washington, Seattle, Washington

(Manuscript received 6 February 2015, in final form 30 March 2016)

ABSTRACT

Satellite radar and radiometer data indicate that subtropical South America has some of the deepest and most extreme convective storms on Earth. This study uses the full 15-yr TRMM Precipitation Radar dataset in conjunction with high-resolution simulations from the Weather Research and Forecasting Model to better understand the physical factors that control the climatology of high-impact weather in subtropical South America. The occurrence of intense storms with an extreme horizontal dimension is generally associated with lee cyclogenesis and a strengthening South American low-level jet (SALLJ) in the La Plata basin. The orography of the Andes is critical, and model sensitivity calculations removing and/or reducing various topographic features indicate the orographic control on the initiation of convection and its upscale growth into mesoscale convective systems (MCSs). Reduced Andes experiments show more widespread convective initiation, weaker average storm intensity, and more rapid propagation of the MCS to the east (reminiscent of the MCS life cycle downstream of lower mountains such as the Rockies). With reduced Andes, lee cyclogenesis and SALLJ winds are weaker, while they are stronger in increased Andes runs. The presence of the Sierras de Córdoba (secondary mountain range east of the Andes in Argentina) focuses convective initiation and results in more intense storms in experiments with higher Andes. Average CAPE and CIN values for each terrain modification simulation show that reduced Andes runs had lower CIN and CAPE, while increased Andes runs had both stronger CAPE and CIN. From this research, a conceptual model for convective storm environments leading to convective initiation has been developed for subtropical South America.

1. Introduction

Convective clouds and midlatitude frontal systems are vital to hydrologic and energy cycles on Earth. As the global climate changes, patterns of severe weather are likely to shift. To eventually include all types of storms in numerical forecasts, high-resolution general circulation models, and climate projections, the physical mechanisms and specific details involving convection initiation, propagation, life cycle, topographical effects, environmental influences, and hydrometeorological impacts from such storms need to be more fully understood. Around the globe, topography on every major continent influences the distribution of precipitation, cloud occurrence and type, climate regimes, convective storms, floods, high-impact weather, hydrometeorology, and much more.

Before the launch of satellites with spaceborne radars, it was difficult to study the physics and characteristics of storms in remote regions. However, radar observations from the Tropical Rainfall Measuring Mission (TRMM) satellite have revolutionized the ability to observe storms in these regions. In the present climate, deep convection tends to form in the vicinity of mountain ranges, and the Andes in subtropical South America help spawn some of the most intense deep convection in the world (Zipser et al. 2006; Houze et al. 2015). On average, South American cloud shields associated with mesoscale convective systems (MCSs) are 60% larger than those over the United States (Velasco and Fritsch 1987), the convection is deeper (Zipser et al. 2006), and they have larger and longer-lived precipitation areas than those over the United States or Africa (Durkee

Corresponding author address: Kristen Lani Rasmussen, National Center for Atmospheric Research, 3450 Mitchell Lane, Boulder, CO 80301.
E-mail: kristenr@ucar.edu

DOI: 10.1175/MWR-D-15-0058.1

et al. 2009). Precipitating systems containing radar echoes of extreme dimension (both vertical and horizontal) are typically associated with the MCS life cycle and contribute ~95% of the climatological warm season rain in the La Plata basin (Rasmussen et al. 2016). The synoptic environment and mechanisms leading to convection with extreme characteristics and MCSs in subtropical South America bear some similarities to those found in other regions of the world, such as the plains east of the Rocky Mountains in the United States, near the western Himalayas in South Asia, and the Sahel region west of the Ethiopian highlands in Africa. These storms are often orogenic, typically originating or occurring near a mountain range.

Over the U.S. Great Plains region, moist low-level flow originating from the Gulf of Mexico is typically capped by warm and dry air flowing off the Mexican Plateau and the Rocky Mountains. This capping inversion inhibits the release of instability over large areas, which by holding at bay the release of the convection ultimately leads to especially intense convective outbreaks in narrowly focused regions where the cap can be broken by a triggering mechanism (Carlson et al. 1983). Velasco and Fritsch (1987), Zipser et al. (2006), and others have pointed out that the topographically guided South American low-level jet (SALLJ; Nogués-Paegle and Mo 1997; Douglas et al. 1998; Saulo et al. 2000; Marengo et al. 2004; Vera et al. 2006) brings moist air poleward and affects the occurrence of intense convection east of the Andes in South America, in a manner somewhat similar to processes east of the Rocky Mountains in the United States. Rasmussen and Houze (2011) used 11 years of TRMM Precipitation Radar (PR) data to show a tendency for squall lines to initiate and develop east of the Andes with a mesoscale organization similar to storms in the U.S. Great Plains. In subtropical South America, however, the topographical influence on the convective initiation and maintenance of the convective systems is unique. Low-level moisture from the Amazon is capped by leeside subsidence of midlevel dry air flowing over the Andes (Rasmussen and Houze 2011). The breaking of the cap and triggering of convection occurs over the Andes foothills and other mountainous terrain of Argentina, just east of the Andes, and MCSs developing from this initiated convection produce damaging tornadoes, hail, and floods across a wide agricultural region east of the mountains to the Atlantic coast (Rasmussen and Houze 2011; Rasmussen et al. 2014).

Cecil (2009, 2011) used TRMM Microwave Imager (TMI) data and ice scattering as a proxy to objectively identify hailstorms and found southeastern South America to be a likely region of large hail production. More recently, Cecil and Blankenship (2012) found that northern Argentina and Paraguay have the highest frequency of significant hail (≥2.5-cm diameter) using AMSR-E data globally. Convective storms with extreme characteristics over subtropical South America also produce significant crop damage and a large number of fatalities, flooding events, and tornadoes (Altinger de Schwarzkopf and Russo 1982; Nascimento and Marcelino 2005; Rasmussen and Houze 2011; Matsudo and Salio 2011; Rasmussen et al. 2014). Thus, subtropical South America is an important yet understudied natural laboratory and socioeconomic venue for investigating the climatological factors controlling severe weather and MCSs near a major mountain range.

In a data-sparse region such as South America, most of the studies of convective systems in this region are derived from satellite radar measurements (Zipser et al. 2006; Romatschke and Houze 2010; Rasmussen and Houze 2011; Rasmussen et al. 2014, 2016). However, information about the underlying storm life cycle, thermodynamic characteristics, and physical processes could not be determined from satellite precipitation radar alone since TRMM only provide snapshots of convective systems. In addition, the lack of widespread and high-resolution surface, upper-air, and operational radar observations in South America[1] limits the investigation and validation of environmental conditions leading to convection with extreme characteristics. To advance the understanding of these storms requires modeling in conjunction with the satellite radar data. This study therefore uses the full 15-yr TRMM PR dataset together with high-resolution model simulations to better understand the physical factors that control the climatology of high-impact weather in subtropical South America and to investigate the storm mechanisms and convective initiation patterns suggested by the TRMM observations. Characterizing the meteorological environment favorable to producing extreme storms will provide insight into the orographic control on convective system life cycle in subtropical South America. For example, the SALLJ and corresponding moisture transport from the Amazon basin is absent without the presence of the Andes (Insel et al. 2010). To investigate the role of topography in convective initiation, we conduct terrain modification experiments that both reduce

[1] Field campaigns have been conducted in South America and limited observational data are available [e.g., TRMM-LBA in the Amazon basin, South American Low-Level Jet Experiment (SALLJEX) in Bolivia, and CHUVA in Brazil], but none have occurred near the foothills of the Andes in western Argentina.

TABLE 1. Number of WCCs in the La Plata basin (38°–27°S, 64°–51°W; black box in Fig. 3f) seen by the TRMM PR from September to February 1998–2013.

Month	No. of WCCs in the La Plata basin
Sep	97
Oct	121
Nov	104
Dec	116
Jan	113
Feb	113

and increase the height of the Andes and various secondary terrain features. The numerical simulations and terrain modification experiments presented herein provide insights into key mechanisms associated with the orographic initiation of deep convection in subtropical South America and improves our understanding of orographic precipitation on a global scale.

2. Methodology and model experimental design

a. TRMM and reanalysis data methodology

This study uses 15 years of V7 TRMM PR data (Iguchi et al. 2000, 2009) obtained during the austral summer (December–February) from 1998 to 2012. The TRMM PR 2A25 data provide three-dimensional volumes of radar reflectivity and rain characteristics (convective, stratiform, or other). The radar data are analyzed using a methodology, developed by Houze et al. (2007), in which an algorithm identifies contiguous three-dimensional echo structures from the TRMM PR data and categorizes them according to whether they contain deep convective cores (DCCs; 40-dBZ echo $\geq$ 10 km in maximum height) or wide convective cores (WCCs; 40-dBZ echo $\geq$ 1000 km^2 when projected onto a horizontal plane). DCCs represent vigorous developing convection and WCCs indicate convection that has organized on the mesoscale. By identifying particular types of extreme echoes in either horizontal or vertical dimensions, this method characterizes precipitating systems by the physical processes occurring within them. However, each echo object identified by the above extreme criteria is embedded within a larger precipitating system that we refer to as a "storm." Storms containing such echo objects represent a particularly extreme subset of the cloud population of South America and will be referred to as "storms with extreme characteristics." This methodology has been employed in previous studies to investigate the global population of convective systems (Houze et al. 2007; Romatschke and Houze 2010; Houze et al. 2011; Rasmussen and Houze 2011; Zuluaga and Houze 2013; Rasmussen et al. 2013, 2014, 2015, 2016; Houze et al. 2015). The probability of finding both types of convective echo features in South America was shown in Romatschke and Houze (2010) and has been updated to include the entire TRMM dataset and austral spring in Rasmussen et al. (2016).

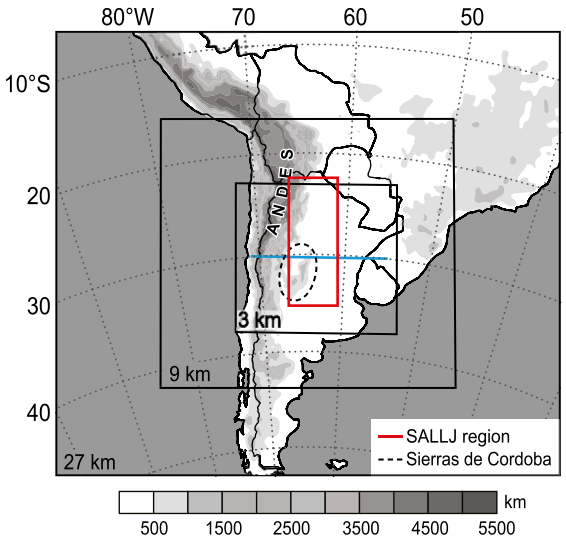

FIG. 1. Domains used in the WRF simulations, centered over Argentina and the Sierras de Córdoba Mountains (shown in the dashed black line). Topography is indicated in the grayscale shading. All simulations used the following domain setup: 1) domain 1: outer domain with a 27-km horizontal resolution and 209 × 184 grid points, 2) domain 2: nested domain with a 9-km horizontal resolution with 374 × 341 grid points, and 3) domain 3: inner domain with a 3-km horizontal resolution and 614 × 563 grid points. The region outlined with the red line represents the SALLJ region used for averaging in Tables 4–6 and Fig. 17. The blue line indicates the location of the cross sections in Fig. 14.

The main objective of this study is to investigate the relationship between the Andes orography and convective initiation of systems that sometimes grow upscale to form MCSs. Rasmussen and Houze (2011) showed that of the types of storms with extreme characteristics identified by the above criteria, storms containing WCCs are the most numerous in the La Plata basin. They produce large volumetric rainfall consisting of both convective and stratiform components and are associated with low-level counterclockwise wind shear related to the SALLJ. The previous studies of Romatschke and Houze (2010), Rasmussen and Houze (2011), and Zuluaga and Houze (2013) have shown that storms containing WCCs represent the developing and mature stage of convective systems that have organized on the mesoscale but not yet reached their ultimate mature stage. Thus, the meteorological environments that favor the development of storms containing WCCs represent an important crucial subset of the high-impact weather in subtropical South America relevant to this study.

TABLE 2. WRF Model setup for all simulations.

Physical process	Scheme	Reference
Longwave radiation	Rapid Radiative Transfer Model	Mlawer et al. (1997)
Shortwave radiation	Dudhia	Dudhia (1989)
Cumulus convection	Kain–Fritsch, none in domain 3	Kain and Fritsch (1993)
Surface layer	Monin–Obukhov	
Microphysics	Thompson scheme; 6-class scheme with graupel, double moment for cloud ice	Thompson et al. (2008)
Land surface	Noah land surface model	Chen and Dudhia (2001)
Planetary boundary layer	Yonsei University (YSU) PBL	Hong et al. (2006)

We use the National Centers for Environmental Prediction–National Center for Atmospheric Research (NCEP–NCAR) reanalysis data (Kalnay et al. 1996) to create synoptic composite maps of the meteorological conditions on days when the TRMM PR identified a WCC in the La Plata basin (38°–27°S, 64°–51°W) during the austral summer (DJF). A summary of the monthly occurrence of WCCs identified by the TRMM PR (Table 1) shows that similar numbers of cases are observed in the austral spring and summer in the La Plata basin. To provide a greater understanding of the conditions leading up to and following the identification of WCCs in the La Plata basin, time-lagged composites are presented in section 3. Composite fields are computed daily starting 3 days prior to the TRMM-identified WCC to 2 days after. This method characterizes the general conditions leading to and following the occurrence of storms with WCCs in the La Plata basin. Anomalies of the time-lagged fields are computed by subtracting the composite field from the austral summer (DJF) long-term mean reanalysis data (Figs. 3–5) and from December only (Fig. 6).

b. *Mesoscale modeling framework with terrain modifications*

The NCAR Advanced Research Weather Research and Forecasting (ARW-WRF) model, version 3.4.1 (Skamarock et al. 2008), is used to simulate a convective system representative of those examined in the TRMM dataset. This system occurred on 27 December 2003 and contained both a DCC and WCC in its mature phase (WCC $> 15\,000\,\text{km}^2$, DCC $> 16\,\text{km}$). GOES infrared satellite loops show convective initiation along the Andes foothills with subsequent upscale growth as the convective elements aggregated into a robust circular MCS while remaining connected to the terrain on its western edge. This particular case was analyzed in detail in Rasmussen and Houze (2011) and was observed to be of the leading-line/trailing-stratiform archetype (Houze et al. 1990; Houze 2004). In addition, the synoptic conditions of this case study show a baroclinic system passing over the southern Andes (Rasmussen and Houze 2011) similar to the findings from Romatschke and Houze (2010) that found a majority of the WCCs in subtropical South America are associated with relatively strong synoptic forcing. The storm was located in a synoptic-scale region of strong surface convergence, sharp temperature and moisture gradient, and exhibited a leading-line/trailing-stratiform radar-echo structure in the TRMM PR data (Rasmussen and Houze 2011).

The ARW-WRF V3.4.1 model is a compressible, nonhydrostatic, three-dimensional mesoscale model. The model was initialized with GFS data at 0000 UTC 26 December 2003 and run for 48 h using a triple-nested domain of 27, 9, and 3 km (Fig. 1). All of the domains used two-way nesting and each simulation had 40 uneven vertical levels with maximum resolution in the boundary layer. A microphysics ensemble study was first performed to assess which of several available microphysics schemes best captured the TRMM PR data in three-dimensional space (Rasmussen 2014, chapter 6). The Thompson et al. (2008) microphysics scheme best captured the mesoscale structure of the simulated MCSs, including a robust leading line of convection and trailing stratiform precipitation at a mature phase in the storm life cycle. Rozante and Cavalcanti (2008) examined MCS cases from the SALLJEX experiment and concluded that the Kain–Fritsch cumulus parameterization performed well in South America and is used in the current study in domains 1 and 2. A summary of the model architecture and experimental setup used in all simulations is shown in Table 2.

To investigate how changes in the Andes topography and related terrain features influence the convective initiation, intensity, spatial distribution, and character of the simulated convective systems, the model simulations were conducted using six terrain configurations (Fig. 2). The WRF simulations were run using identical input conditions and parameters for the different terrain configurations detailed in Table 3. Reducing the terrain by 50% (low ANDES runs; Figs. 2c,d) provides a comparison of the role of the extreme vertical height of the Andes in convective initiation to lower mountain ranges

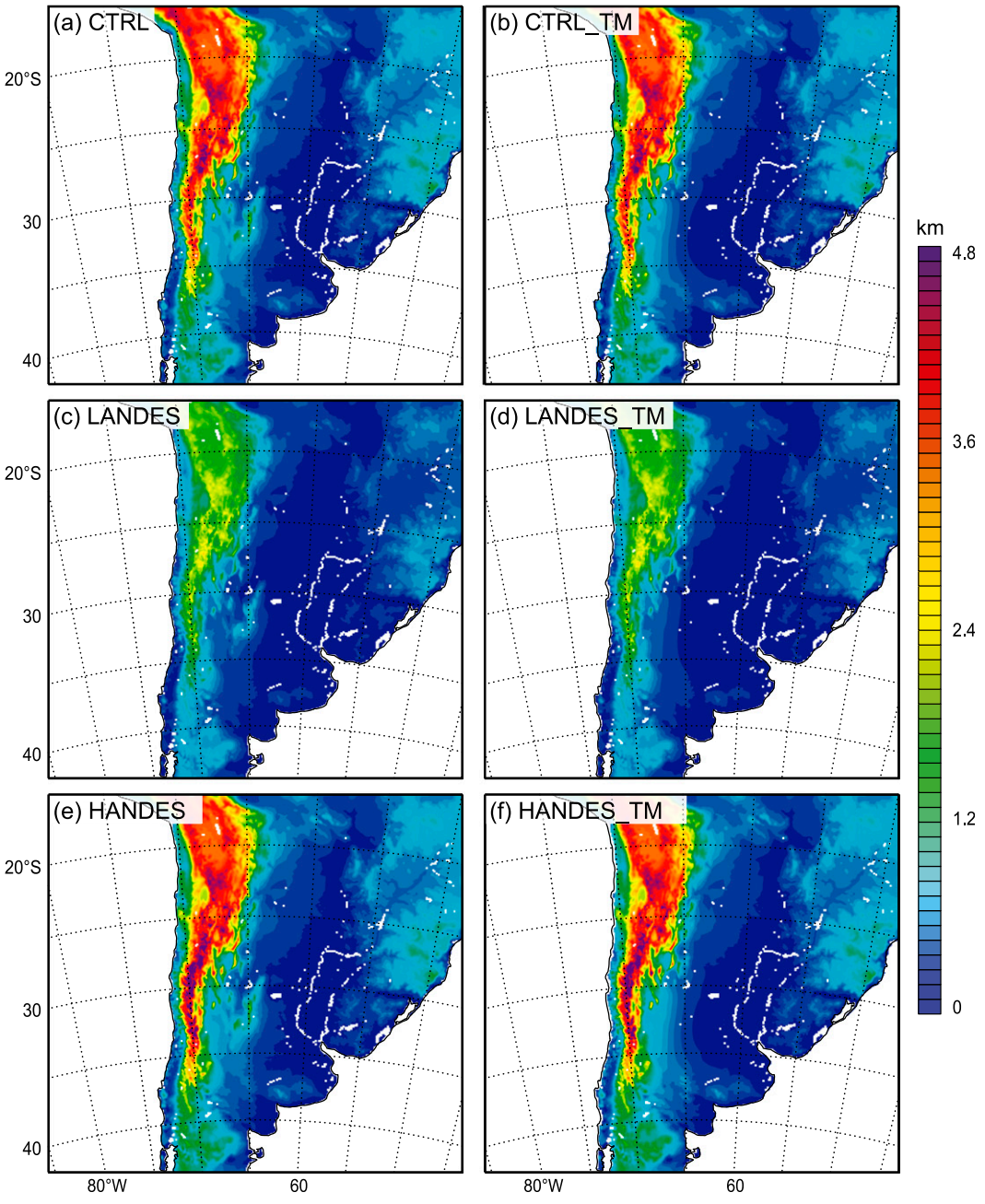

FIG. 2. Topography used for the WRF terrain modification simulations: (a) control experiment, no modifications (CTRL); (b) Sierras de Córdoba (SC) mountains removed from the CTRL terrain (CTRL_TM); (c) CTRL terrain reduced by 50% (LANDES; Low Andes); (d) SC mountains removed from the LANDES terrain (LANDES_TM); (e) CTRL terrain increased by 20% south of 26.5°S (HANDES; High Andes); and (f) SC mountains removed from the HANDES terrain (HANDES_TM).

around the world with similar orientation relative to the low-level moisture flow (especially the Rocky Mountains). Increasing the southern Andes by 20% (high ANDES runs; Figs. 2e,f) allows for an analysis of the relationship between the low-level synoptic waves passing over the southern Andes and the degree of modification experienced by these features in the presence of a larger mountain range. Increased terrain heights in the southern Andes provide greater flow-modification effects through a deeper layer in the lower troposphere and the resulting influence on the convective systems in the lee are examined. Finally, all three

TABLE 3. WRF terrain modification experiment summary.

Simulation name	Terrain modifications
CTRL	None; original terrain
CTRL_TM; CTRL topography with terrain modification (TM)	Sierras de Córdoba (SC) mountains removed only
LANDES; low Andes	50% reduction in CTRL terrain
LANDES_TM; low Andes with terrain modification (TM)	LANDES without SC mountains
HANDES; high Andes	20% increase in the Andes from the CTRL terrain south of 26.5°S
HANDES_TM; high Andes with terrain modification (TM)	HANDES without SC mountains

major Andes height configurations were run without the Sierras de Córdoba Mountains (Figs. 2b,d,f) to investigate the role of this small secondary mountain range that has been hypothesized to help focus deep convective initiation in a narrow region in subtropical South America (Romatschke and Houze 2010; Rasmussen and Houze 2011).

As will be described in section 4b, a storm-tracking algorithm was developed for this study. At each simulation time, grid elements that contained values exceeding a certain threshold are identified. The latitude and longitude coordinates of those grid boxes are averaged to get a domain-scale average of where those values were located. This technique is different from traditional storm-tracking algorithms because this study is concerned with cloud populations and not necessarily individual storm movement.

c. *Moisture flux convergence*

Moisture flux convergence is a valuable tool in assessing the atmospheric environment leading to convective initiation (Banacos and Schultz 2005). Following the method described in Banacos and Schultz (2005), moisture flux convergence was calculated in the terrain modification simulations. Moisture flux convergence (MFC) is a combination of moisture advection and convergence terms shown in Eq. (1) below, where u and v are zonal and meridional winds and q is specific humidity:

$$\mathrm{MFC} = \underbrace{-u\frac{\partial q}{\partial x} - \frac{\partial q}{\partial y}}_{\text{advection}} \underbrace{- q\left(\frac{\partial u}{\partial x} + \frac{\partial v}{\partial y}\right)}_{\text{convergence}} . \qquad (1)$$

Values of MFC, $\mathrm{MFC_{adv}}$, and $\mathrm{MFC_{conv}}$ were calculated for the terrain modification simulations and the results are presented in Table 6.

3. Synoptic evolution of convective storm environments

To obtain an understanding of the occurrence of synoptic-scale patterns related to convective storm initiation and development, time-lagged reanalysis composites associated with TRMM-identified WCCs in subtropical South America are presented in this section. Figure 3 shows a time-lagged sequence of composite 850-hPa (color contours) and 500-hPa (gray contours) geopotential height anomalies relative to the occurrence of a TRMM-identified WCC (labeled day 0; Fig. 3d) in the La Plata basin (38°–27°S, 64°–51°W). When TRMM-identified storms containing WCCs are located in the La Plata basin, the low-level pressure field exhibits significant flow modification while traversing the southern Andes Mountains (Figs. 3a–c). The Andes have an average altitude of ~4 km, but the average height decreases to the south. The midlatitude synoptic features at low levels traverse the mountains and likely experience flow modification consistent with similar situations in other regions of the world influenced by large mountain ranges (e.g., the Rocky Mountains, East Asian mountains, southern Alberta, and the European Alps; Chung 1977). The development of the low-level pressure field on the eastern side of the Andes resembles the canonical lee cyclogenesis scenario that is frequently observed in the lee of the Rocky Mountains and other major mountain ranges (Smith 1984, 1986; Davis 1997; Schultz and Doswell 2000). Some previous studies have documented the lee cyclogenesis effect east of the Andes Mountains (Chung 1977; Satyamurty et al. 1990; Gan and Rao 1994), but Fig. 3 establishes a connection between lee cyclogenesis and storms containing WCCs that typically manifest as MCSs with significant precipitation and severe weather over Argentina (Rasmussen et al. 2014, 2016).

The deepest 850-hPa low in the composite maps is concurrent with storms containing WCCs (Fig. 3d). Deep lee cyclogenesis occurs primarily from the atmospheric dynamics related to the westward-tilted upper- and low-level pressure anomalies (Palmén and Newton 1969). When a synoptic wave encounters topography, it weakens, decelerates, and moves poleward (Davis 1997; Schultz and Doswell 2000). As the tropospheric air traverses the topography, a lee trough develops (typically equatorward of its original latitude) in response to adiabatic warming from dry air descent (Davis 1997; Schultz and Doswell 2000), represented by the pressure

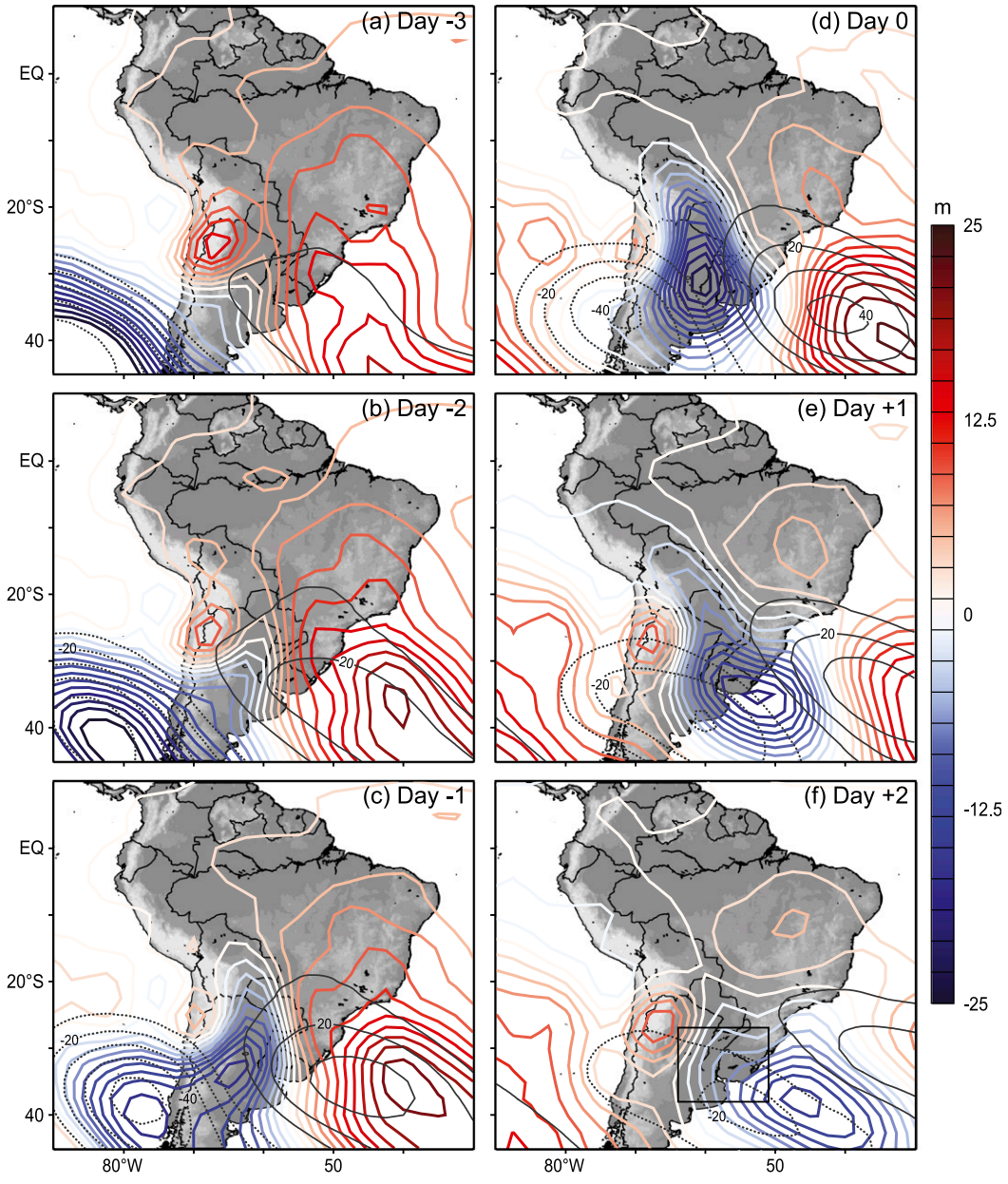

FIG. 3. Time-lagged climatological composite maps for days on which the TRMM PR identified storms containing wide convective cores over the La Plata basin [38°–27°S, 64°–51°W; black box in (f)] in the austral summer (DJF) for (a) day −3, (b) day −2, (c) day −1, (d) day 0, (e) day +1, and (f) day +2. The 850- and 500-hPa geopotential height anomalies are represented by color and gray contours (dashed contours represent negative values), respectively. The composites are composed of 342 days.

pattern sequence in Fig. 3. Positive thermal anomalies in the lee of mountains (Buzzi and Tibaldi 1978) provide a thermally direct circulation that converts eddy potential energy into eddy kinetic energy, indicative of the baroclinic component of the developing lee trough (McGinley 1982).

In addition to the presence of lee cyclogenesis, Fig. 4 shows a clear relationship between the SALLJ and the occurrence of storms containing WCCs. Three days prior to the occurrence of storms containing WCCs in the La Plata basin, the meridional wind strength related to the SALLJ (colored contours in Fig. 4) was only slightly higher than normal. However, in the two subsequent days prior to the WCC occurrence, the strength of the SALLJ became notably stronger (~twice as large as the climatological wind speed), thus producing

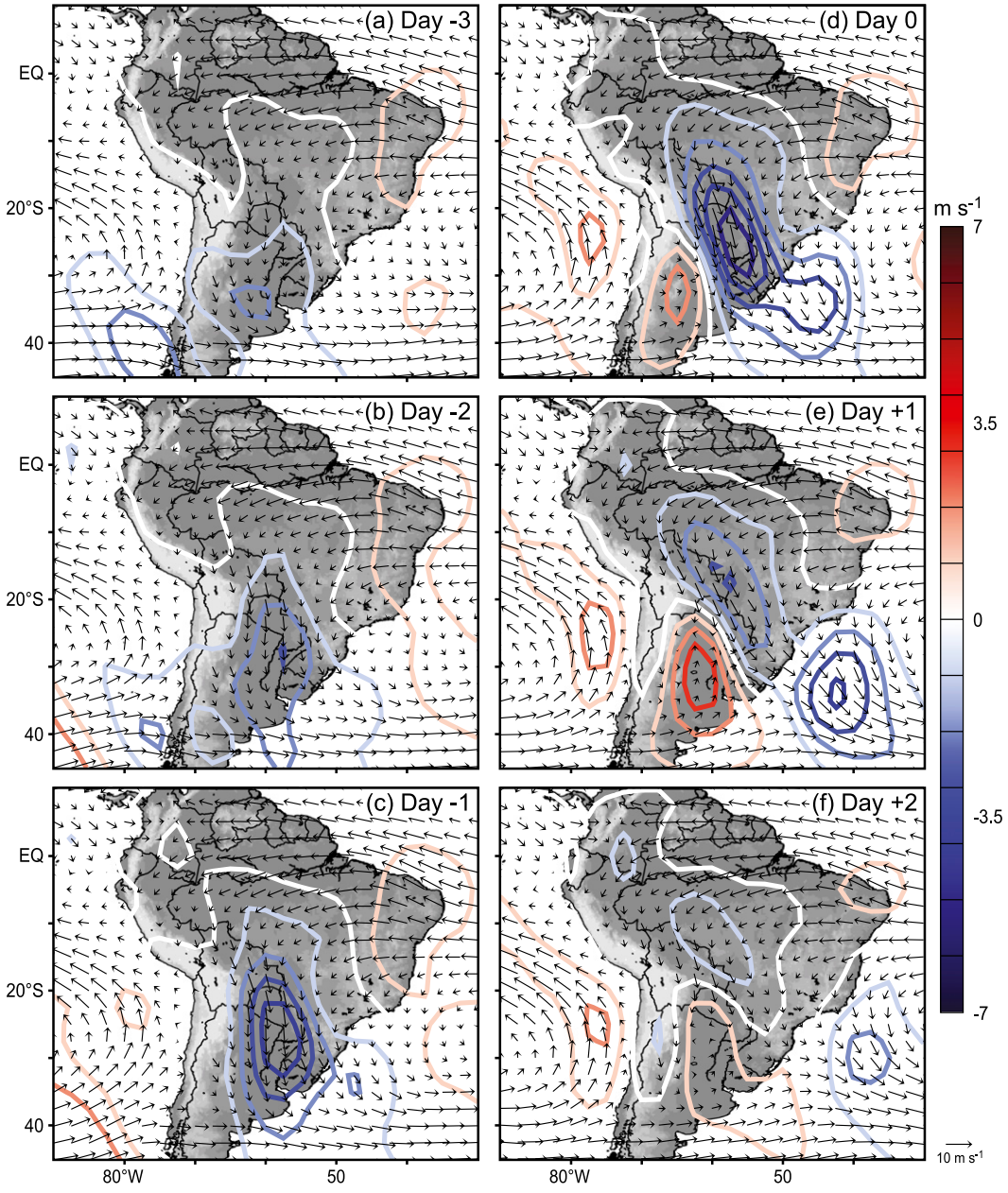

FIG. 4. As in Fig. 3, but for 850-hPa meridional wind anomalies ($m\,s^{-1}$) represented by the colored contours. Black composite horizontal 850-hPa full winds (vectors) are shown for comparison.

stronger moisture and warm temperature advection from the Amazon basin (Fig. 5). Because a strong cyclone was developing in the lee of the Andes at the same time (Fig. 3), a notable north–south pressure gradient along the eastern foothills of the Andes strengthened the SALLJ through downgradient suction effects. The strengthened SALLJ increased the available moisture and therefore the low-level instability required for convective storms with extreme characteristics in the region (Fig. 5). The robust signals in the composite maps (Figs. 3 and 4) show the baroclinic wave trough in the westerlies and its baroclinic environment with cyclogenetic tendencies and northerly prefrontal low-level jet (Emanuel et al. 1987; Houze 2014, chapter 11) being reinforced by lee cyclogenesis induced by the Andes and the SALLJ channeled southward parallel to the mountains. The meridional wind anomalies associated with the deep lee cyclone resulted in strong southerly flow along

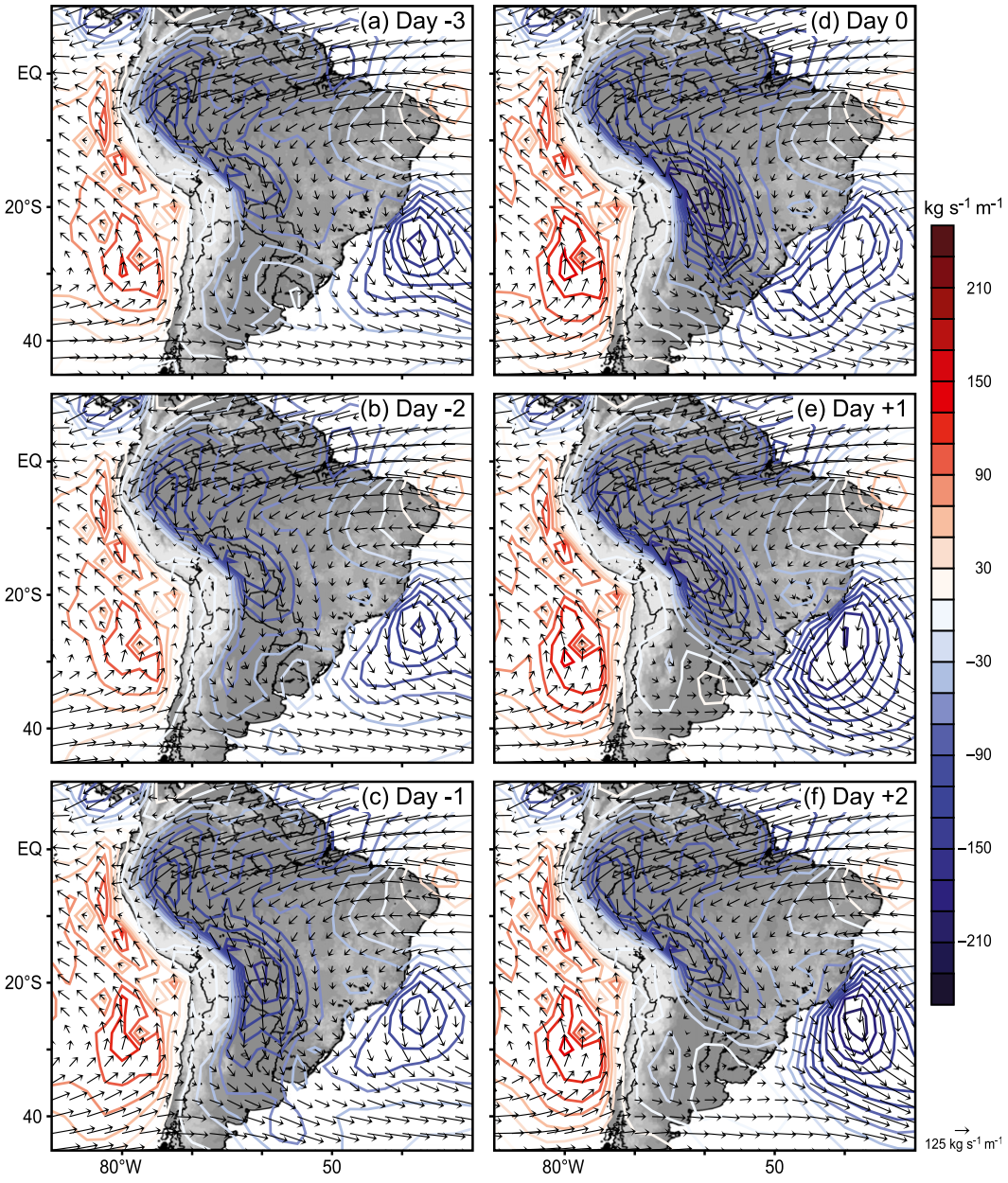

FIG. 5. As in Fig. 3, but for integrated meridional moisture flux (kg s^{-1} m^{-1}) represented by the colored contours. Black full integrated moisture flux vectors (kg s^{-1} m^{-1}) are shown for comparison.

the Andes foothills (Figs. 4d,e) and created a strong zone of convergence that provided continued forcing for the longer-lived MCSs to develop and grow upscale.

The relationship between an enhanced SALLJ and convective storm occurrence was previously noted by Salio et al. (2007), but their study did not discuss why an increased SALLJ occurs in conjunction with convective storms. However, composite analysis of days when TRMM observed WCCs in the La Plata basin shows that the influence of the Andes on the environment favorable for widespread and strong convection in subtropical South America results in the modification of the existing baroclinic wave circulation as it moves across the mountains. This inference will be tested by the numerical modeling experiments presented in the next section. Although some differences exist, Fig. 6 shows that the simulated storm is typical of those represented by the composite analysis of Figs. 3–5. Therefore, the model results are likely representative of an important class of storms over the La Plata basin.

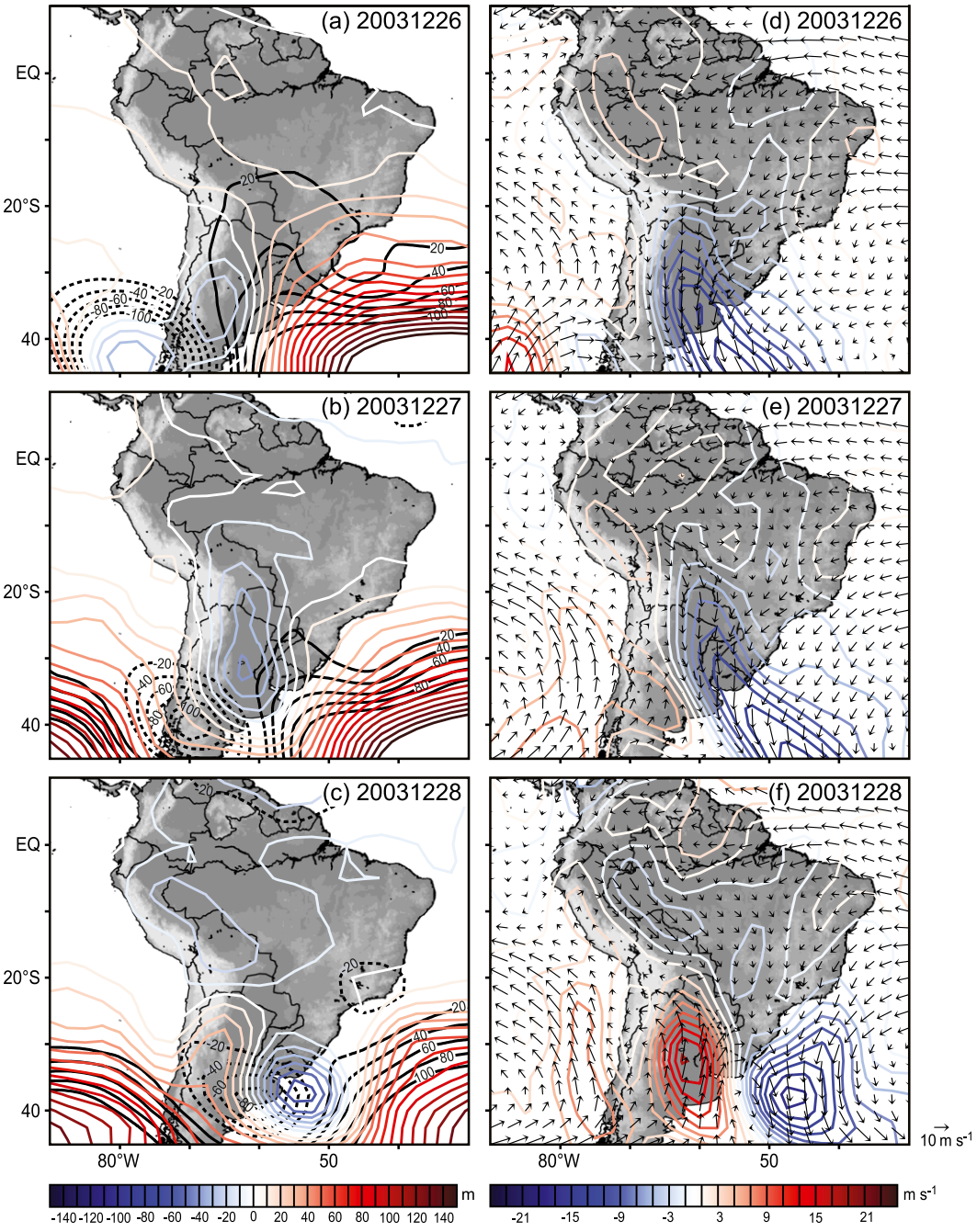

FIG. 6. Synoptic maps for 26–28 Dec 2003 for (a)–(c) 850- and 500-hPa geopotential height anomalies (m) and (d)–(f) 850-hPa meridional wind anomalies (m s^{-1}) and 850-hPa full winds (vectors) in the same style as in Figs. 3 and 4, respectively. The anomalies are calculated based on the December climatology.

4. Storm behavior as a function of terrain configuration

a. The suite of experiments

To further probe the relationship between the Andes and the life cycle of the convective storm examined here, terrain modification experiments were performed as described in section 2 and shown in Fig. 2. Six different terrain configurations used in the WRF simulations are summarized in Table 3 and these simulation names will be used throughout the rest of the manuscript. Three main types of modifications were conducted, including reducing and increasing the height of the Andes Mountains, and removing the secondary mountain range east of the

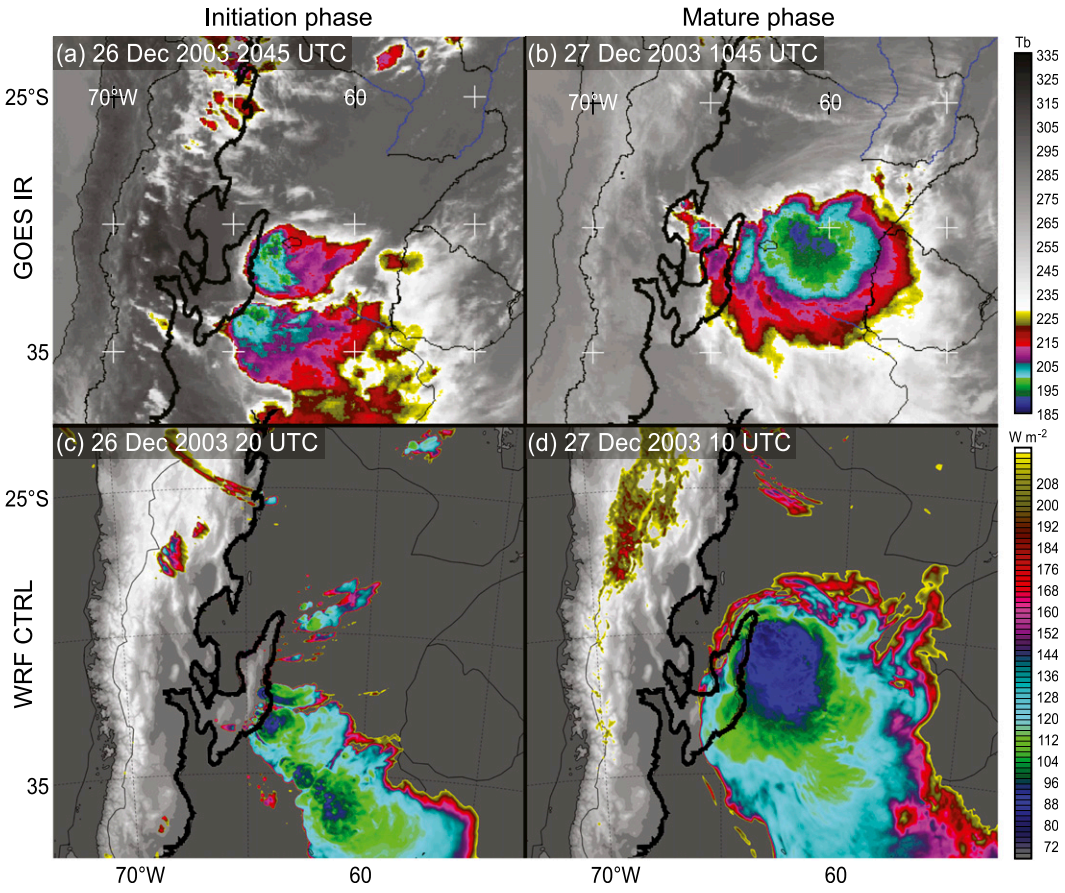

FIG. 7. Comparisons of the GOES infrared satellite data to the WRF CTRL simulations at an early initiation phase and a later mature phase of the storm life cycle. The panels show the following: (a) GOES IR brightness temperatures (K) at 2045 UTC 26 Dec 2003; (b) as in (a), but at 1045 UTC 27 Dec 2003; (c) WRF CTRL simulation outgoing longwave radiation (OLR; W m^{-2}) at 2000 UTC 26 Dec 2003; and (d) as in (c), but at 1000 UTC 27 Dec 2003. The thick black outline in all panels represents the 0.5-km topography for reference.

Andes (Sierras de Córdoba Mountains). The resulting suite of numerical experiments enables an analysis of the impact of both large and small-scale variations in topography in generating and organizing convective storms in the lee of the Andes.

b. *Model MCSs compared with satellite data*

Figure 7 shows a comparison of the GOES infrared satellite brightness temperatures and control (CTRL) simulation outgoing longwave radiation (OLR; W m^{-2}) at key times in the mesoscale storm development. OLR serves as a proxy for the temperature and height of the upper-level cloud shield in deep convective systems as was shown to be a reasonable approximation for deep convection by Gutzler and Wood (1990). At an early stage associated with convective initiation (Figs. 7a and 7c), the observed and modeled storms occur in a similar location on the eastern foothills of the Sierras de Córdoba Mountains at a comparable time, providing confidence in the model representation of convective initiation in this region. Similarly, when the convective system had become more organized and grown upscale into a mature MCS (Figs. 7b and 7d), both the GOES-IR and model OLR fields show a deep circular cloud shield attached to the northeastern edge of the Sierras de Córdoba Mountains. However, notable departures from the observations are seen in the southeast extension of the cloud features at both times. Figure 8 shows a comparison between the TRMM PR data and model reflectivity (dBZ) at the mature phase of the MCS in both horizontal and vertical perspectives. The leading-line/trailing-stratiform structure is clearly seen in both the observations and CTRL model simulation. Although differences exist between the TRMM data and simulated storm, a detailed microphysics sensitivity test revealed that the Thompson scheme best reproduced the horizontal and vertical structures of convective and stratiform precipitation observations

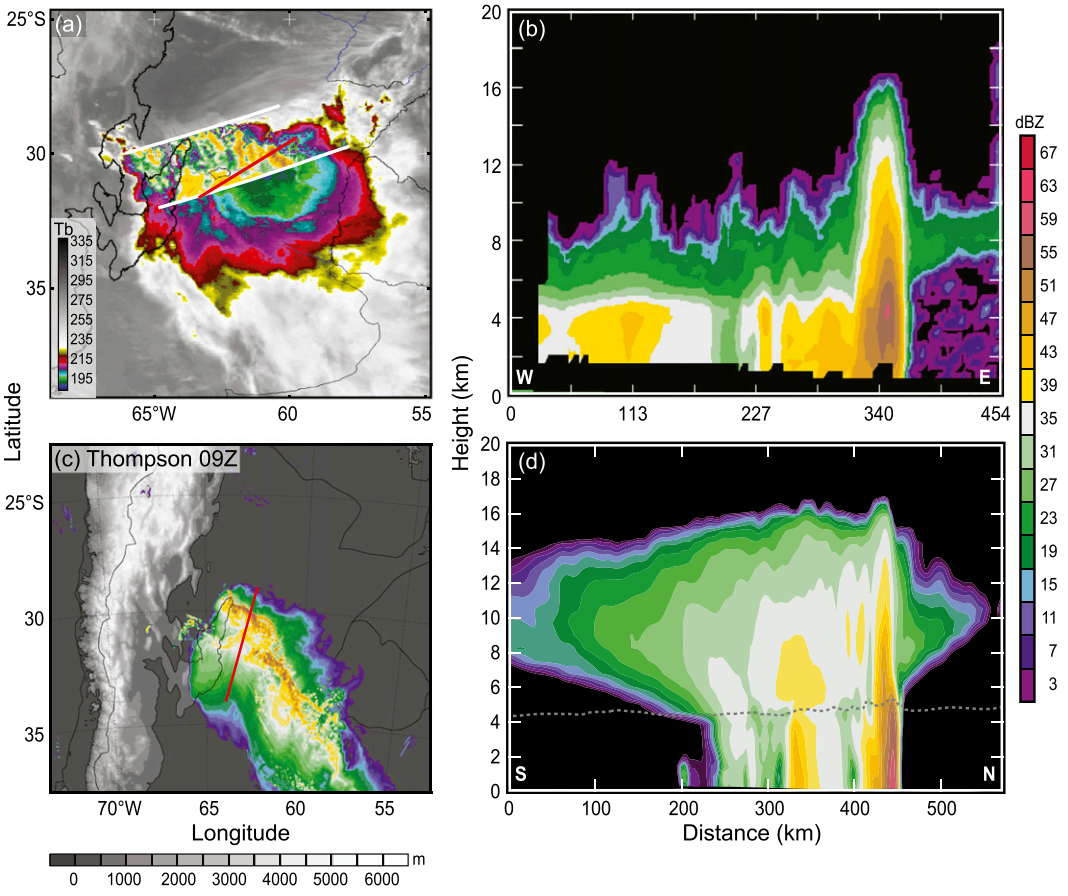

FIG. 8. Horizontal and vertical cross-sectional comparisons of TRMM PR data and the WRF CTRL simulations. (a) Reflectivity from the TRMM PR in dBZ at 4 km at 1000 UTC 27 Dec 2007 overlaid on the IR satellite brightness temperature (K). The white lines indicate the TRMM PR swath and the red line indicates the location of the (b) vertical cross section. (c) Reflectivity from the WRF CTRL simulations at 4 km at 0900 UTC 27 Dec 2003 and (d) the corresponding cross sections from its horizontal representation along the red line in (c). The thick black contour outlines the 0.5-km topography in (a) and (c). In (d), the gray dashed line represents the 0°C level.

(Rasmussen 2014). Thus, we posit that the terrain modification experiments provide a reasonable test of how various configurations of orography impact the resulting convective storm initiation, upscale growth, and development.

c. *Lee cyclogenesis and the strength of the SALLJ*

Convective initiation typically occurs ahead of a cold frontal passage in the presence of strong northerly moisture flux from the Amazon basin (Fig. 5). In this section, we test the hypothesis that the presence of a taller mountain range creates greater modification of the flow pattern as low-level synoptic features traverse the range, leading to a deeper lee cyclone. Figure 9 presents 850-hPa geopotential height difference maps compared to the CTRL simulation for each of the five terrain modification experiments. Slight differences between the reanalysis and model representations of lee cyclogenesis in this region could potentially impact the results, but the dominant features are present in the model (Fig. 9a) in comparison with the 850-hPa geopotential heights on 27 December 2003 (not shown). The most robust result is seen in the reduced Andes runs (Figs. 9c and 9d) wherein the lower mountain range produces a weaker lee cyclone compared to the CTRL case. Also notable is that this reduction is largest in the immediate foothills of the Andes, confirming the role of the terrain in the dynamical production of lee cyclogenesis, consistent with the results of many previous studies in other regions of the world (Kasahara 1966; Smith 1984,1986). In contrast, when the southern Andes are increased in height[2] (Figs. 9e,f), the lee cyclone

[2] Note that this increase is not symmetrical with respect to the reduced Andes runs as described in section 2b and Table 2.

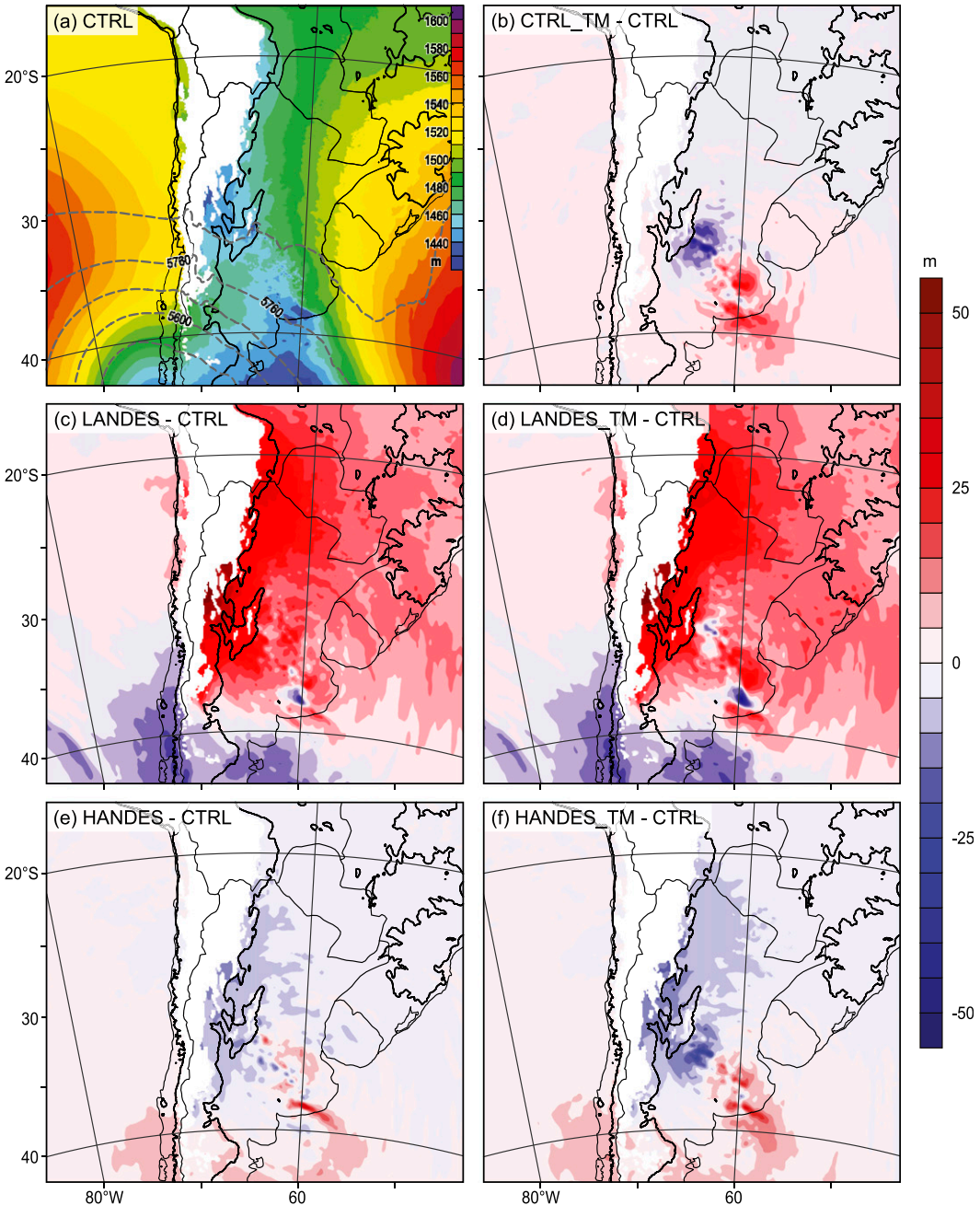

FIG. 9. (a) Map of 850- and 500-hPa geopotential heights (m) in color shading and dashed gray contours, respectively, at 2000 UTC 26 Dec 2003 from the CTRL run. Difference maps of 850-hPa geopotential height (m) from the terrain modification runs compared to the CTRL run in domain 2: (b) CTRL_TM − CTRL, (c) LANDES − CTRL, (d) LANDES_TM − CTRL, (e) HANDES − CTRL, and (f) HANDES_TM − CTRL. Regions where the 850-hPa surfaces intersect the terrain are masked out. The 0.5-km topography in the CTRL run is outlined in black for reference.

deepens, which is consistent with terrain-forced lee cyclogenesis (Schultz and Doswell 2000).

Table 4 presents the time-averaged geopotential height differences (in meters) for all terrain-modification experiments in the SALLJ region shown in Fig. 1. In the LANDES runs, geopotential height differences are significantly lower in magnitude than the CTRL or HANDES runs, echoing the patterns in Fig. 9. In contrast, the HANDES runs are slightly larger in magnitude than the CTRL runs, indicating the role of the higher southern Andes in producing a deeper lee cyclone. Thus, the model results appear to

TABLE 4. Time-averaged geopotential height differences (m) from the CTRL simulation for each terrain modification simulation in the SALLJ region shown in Fig. 1 in domain 2. All values are averaged from hours 6–36 of each simulation.

Run	700-hPa geopotential height diff from CTRL (m)	850-hPa geopotential height diff from CTRL (m)	950-hPa geopotential height diff from CTRL (m)
CTRL_TM	−0.6	−1.0	−3.0
LANDES	12.1	17.9	16.5
LANDES_TM	11.6	17.0	15.1
HANDES	−2.8	−3.2	−2.9
HANDES_TM	−4.2	−5.4	−6.9

confirm the notion that a taller mountain range tends to produce deeper lee cyclogenesis associated with greater flow modification along higher terrain, consistent with Fig. 3.

To further investigate the impact of the orography on the behavior and strength of the SALLJ related to convective storms in this region, analysis of the time-averaged meridional winds, integrated meridional moisture flux, and MFC in the SALLJ region (Fig. 1) are presented in Tables 5 and 6. The LANDES runs show a significant decrease in northerly meridional wind strength, especially at lower levels (e.g., 950 and 850 hPa) that are typically associated with the height of the strongest SALLJ magnitude (between ~1000–1600 m MSL; Douglas et al. 1998; Vera et al. 2006). The vertically integrated meridional moisture flux magnitude also decreases with lower Andes (Table 6). Large decreases of MFC, MFC_{adv}, and MFC_{conv} with a lower Andes compared to the CTRL run (reduced by 22.7%, 63.8%, and 11.8%, respectively; Table 6) indicate that less moisture was available for convection and likely resulted in lower convective available potential energy (CAPE), as will be shown in section 4h. These results are consistent with recent work by Insel et al. (2010), who used a regional climate model to conduct reduced Andes topography experiments and showed a significant reduction and absence of the SALLJ in simulations with 50% and 0% Andes configurations, respectively. The lower mountains produce less mechanical forcing on the lower levels of the atmosphere. In addition, a weaker lee cyclone results in a weaker north–south pressure gradient force and therefore a weaker SALLJ, vertically integrated meridional moisture flux, and MFC (decrease is particularly noteworthy in the MFC_{adv} component). Thus, it seems that the combination of enhanced flow modification leading to deeper lee cyclogenesis and a stronger north–south pressure gradient force are intimately related to the height and characteristics of the mountain barrier that control the response in the lee and help modulate the convective storm environment and the resulting storm life cycle development in South America.

d. Convective initiation and early growth

Figure 7 shows that at an early initiation time in the simulations, the CTRL run resembles the observational GOES IR data in both temporal and spatial perspectives. Figures 10 and 11 present OLR difference plots compared to the CTRL run for each of the terrain modification experiments. When the Andes are unchanged, but the Sierras de Córdoba are removed (CTRL_TM; Fig. 10a), convective initiation is less focused along the eastern foothills of the Sierras de Córdoba than the simulation with the Sierras de Córdoba. Although the response is complex, it generally agrees with the hypothesis from Romatschke and Houze (2010) and Rasmussen and Houze (2011) discussed in section 2b. However, in the evolution of the convective system with the Sierras de Córdoba Mountains removed (CTRL_TM), a storm system nevertheless occurs, but with less overall convective storm intensity (a point discussed further in section 4g).

TABLE 5. Time-averaged meridional winds ($m\,s^{-1}$) in each terrain modification simulation in the SALLJ region shown in Fig. 1 in domain 2. All values are averaged from hours 6–36 of each simulation.

Run	700-hPa SALLJ (V; $m\,s^{-1}$)	850-hPa SALLJ (V; $m\,s^{-1}$)	950-hPa SALLJ (V; $m\,s^{-1}$)	SALLJ: surface–600 hPa (V; $m\,s^{-1}$)
CTRL	−3.5	−4.5	−4.0	−3.46
CTRL_TM	−3.3	−4.1	−3.6	−3.2
LANDES	−3.4	−2.8	−1.5	−2.0
LANDES_TM	−3.3	−2.5	−1.1	−1.8
HANDES	−3.9	−5.1	−4.7	−3.9
HANDES_TM	−3.7	−4.9	−4.6	−3.8

TABLE 6. Time-averaged vertically integrated moisture flux ($kg\,s^{-1}\,m^{-1}$) in each terrain modification simulation in the SALLJ region shown in Fig. 1 in domain 2. All values are averaged from hours 6–36 of each simulation.

Run	Integrated meridional moisture flux ($kg\,s^{-1}\,m^{-1}$)	MFC (surface–600 hPa; $10^{-4}\,g\,kg^{-1}\,s^{-1}$)	MFC_{adv} (surface–600 hPa; $10^{-4}\,g\,kg^{-1}\,s^{-1}$)	MFC_{conv} (surface–600 hPa; $10^{-4}\,g\,kg^{-1}\,s^{-1}$)
CTRL	−32.11	0.22	0.047	0.17
LANDES	−29.96	0.17	0.017	0.15
HANDES	−32.36	0.24	0.055	0.18

The largest difference in convective initiation is observed in the runs with the Andes reduced by 50% (LANDES; Figs. 10b,c). Convective initiation occurs in a widespread band that extends north into Paraguay and northern Argentina that is not observed in the CTRL run (Figs. 10b and 10c). Rasmussen and Houze (2011) hypothesized that lee subsidence from the midlevel westerlies traversing the Andes provides a capping inversion of warm and dry air between ~20° and 30°S around 700 hPa, preventing low-level instability from releasing until it reaches the Sierras de Córdoba to the south. Rasmussen and Houze (2011) and Rasmussen et al. (2014) discuss the role of the Sierras de Córdoba in focusing deep convection by providing an orographic lifting mechanism for the low-level unstable air to overcome convective inhibition. When the Andes are reduced to half their height in this study (Figs. 10b,c), convectively unstable air is more readily released with the lower mountain range. Increasing the southern Andes height by 20% generally shifts the convective initiation to the south (Figs. 10d,e), in response to the deeper lee cyclone, stronger SALLJ, and associated southward location of the region of convergence (noted in section 3), although the response is complex and should be further examined in future work.

e. *Upscale growth*

Corresponding to a mature phase of the convective storm life cycle shown in Figs. 7b and 7d, OLR difference plots for the terrain modification experiments are presented in Fig. 11 to gain insight into the role of terrain variations in upscale convective growth. The CTRL_TM storm location is relatively similar to the CTRL run, indicating that the presence of the Sierras de Córdoba do not tie the convective storms to the terrain in a general sense (Fig. 11a). Stronger orographic controls are observed in the simulations with 50% reduced Andes terrain (Figs. 11b and 11c). With the reduced Andes, the mature systems are located farther northeast than the CTRL run, reminiscent of the typical MCS life cycle in the United States where the north–south mountain barrier is lower. Weaker lee cyclogenesis and reduced SALLJ magnitude combine to produce an environment that favors convective systems that propagate downstream from the mountain barrier more rapidly than for similar systems downstream of higher mountains (Fig. 11), although intricacies of this relationship should be examined in future work. Increasing the southern Andes by 20% results in a southwestward shift of the convective systems (Figs. 11d and 11e), indicating the robust orographic control on MCSs in this region.

f. *Storm tracks*

To further investigate the relationship between orographic height and convective initiation, Fig. 12 shows the results of a storm-tracking algorithm that identifies the average location of intense values of reflectivity and cloud-top temperatures (description in section 2). For simplicity, only the CTRL and LANDES runs are presented. Identifying regions with particularly intense reflectivity (dBZ) or cloud-top temperature values is a commonly used technique in research around the world on convection seen by satellites (e.g., Zipser et al. 2006; Houze et al. 2007; Yuan and Houze 2010; Zuluaga and Houze 2015; Rasmussen et al. 2014, 2015, 2016; Houze et al. 2015). For the analysis in Fig. 12a, the reflectivity threshold is 45 dBZ to capture the evolution of particularly intense storms. The reduced Andes simulation tends to have average reflectivity ≥45 dBZ farther north compared to the regular Andes terrain (Fig. 12a). Additionally, the LANDES storm track exhibits more northeastward movement of intense convective elements compared to the CTRL, especially from hours 12–24 in Fig. 12a, which is consistent with the discussion above related to Figs. 10 and 11. Comparisons between the storm tracks of the CTRL and LANDES terrain modification simulations with OLR values ≤90 $W\,m^{-2}$ (Fig. 12b) also indicate a farther northeastward average location of the LANDES storm elements. The role of the barrier height in producing deep cold cloud tops closer to the mountain front is also apparent in Fig. 12b. With a lower Andes height, the LANDES storm track originates ~2° longitude east compared to the CTRL storm track in Fig. 12b.

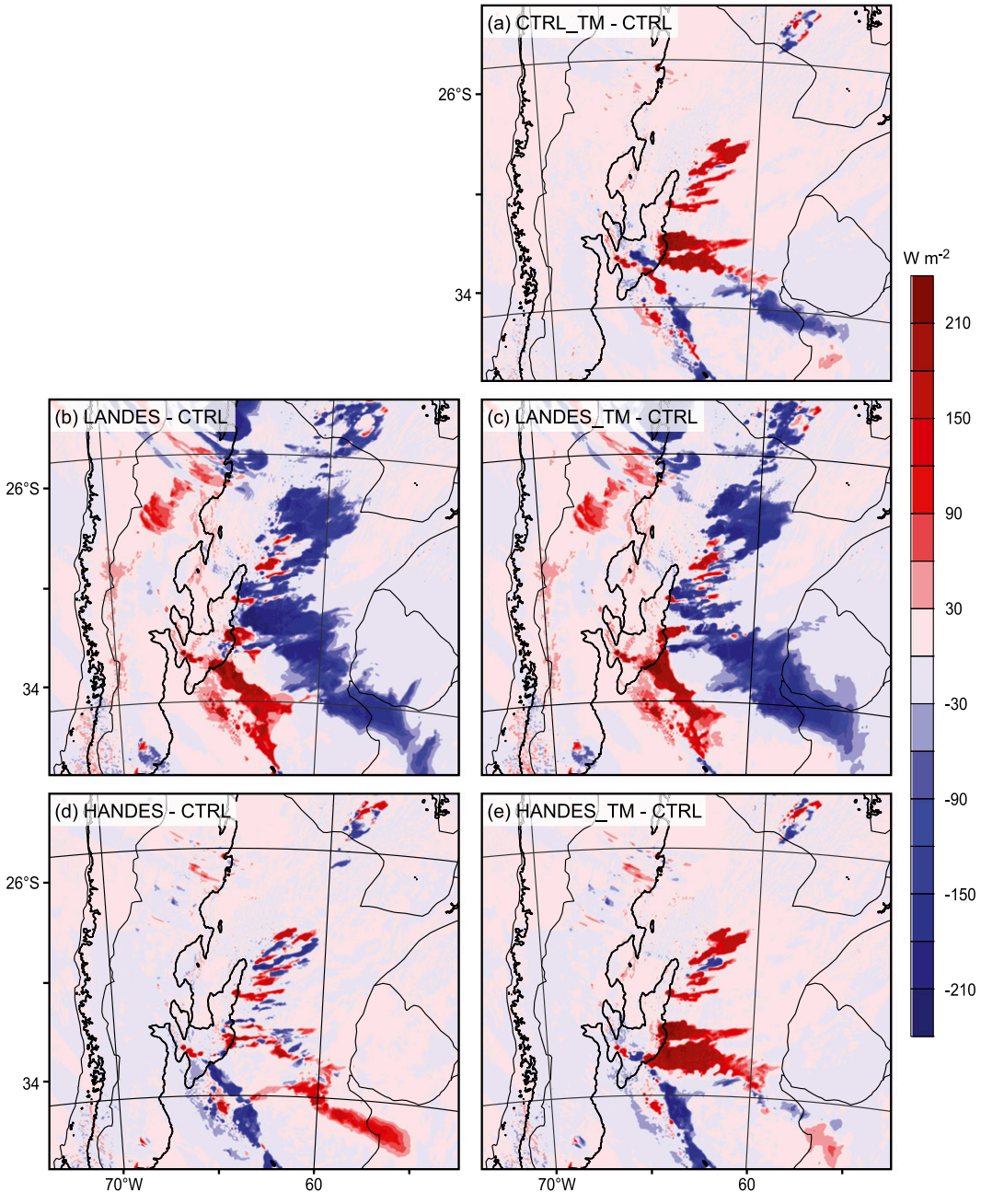

FIG. 10. Difference maps of OLR (W m^{-2}) from the terrain modification runs minus the CTRL run at 2000 UTC 26 Dec 2003 in domain 2: (a) CTRL_TM − CTRL, (b) LANDES − CTRL, (c) LANDES_TM − CTRL, (d) HANDES − CTRL, and (e) HANDES_TM − CTRL. The 0.5-km topography in the CTRL run is outlined in black for reference.

g. *Storm intensity*

To examine the domain-scale effect of varying the topography and intensity of the resulting storms, Fig. 13 presents storm intensity information for the duration of each terrain modification simulation in domain 2 (Fig. 1). The 40-dBZ echo-top heights and occurrences were calculated in each grid box and either averaged (Fig. 13a) or counted (Fig. 13b) from hours 6–36 of each simulation. During the early period of convective activity in each simulation, the 40-dBZ echo tops were higher on average in the CTRL and HANDES runs, which both include the Sierras de Córdoba Mountains (Fig. 13a), indicating their role in focusing deep convection hypothesized in previous studies (Romatschke and Houze 2010; Rasmussen and Houze 2011). In

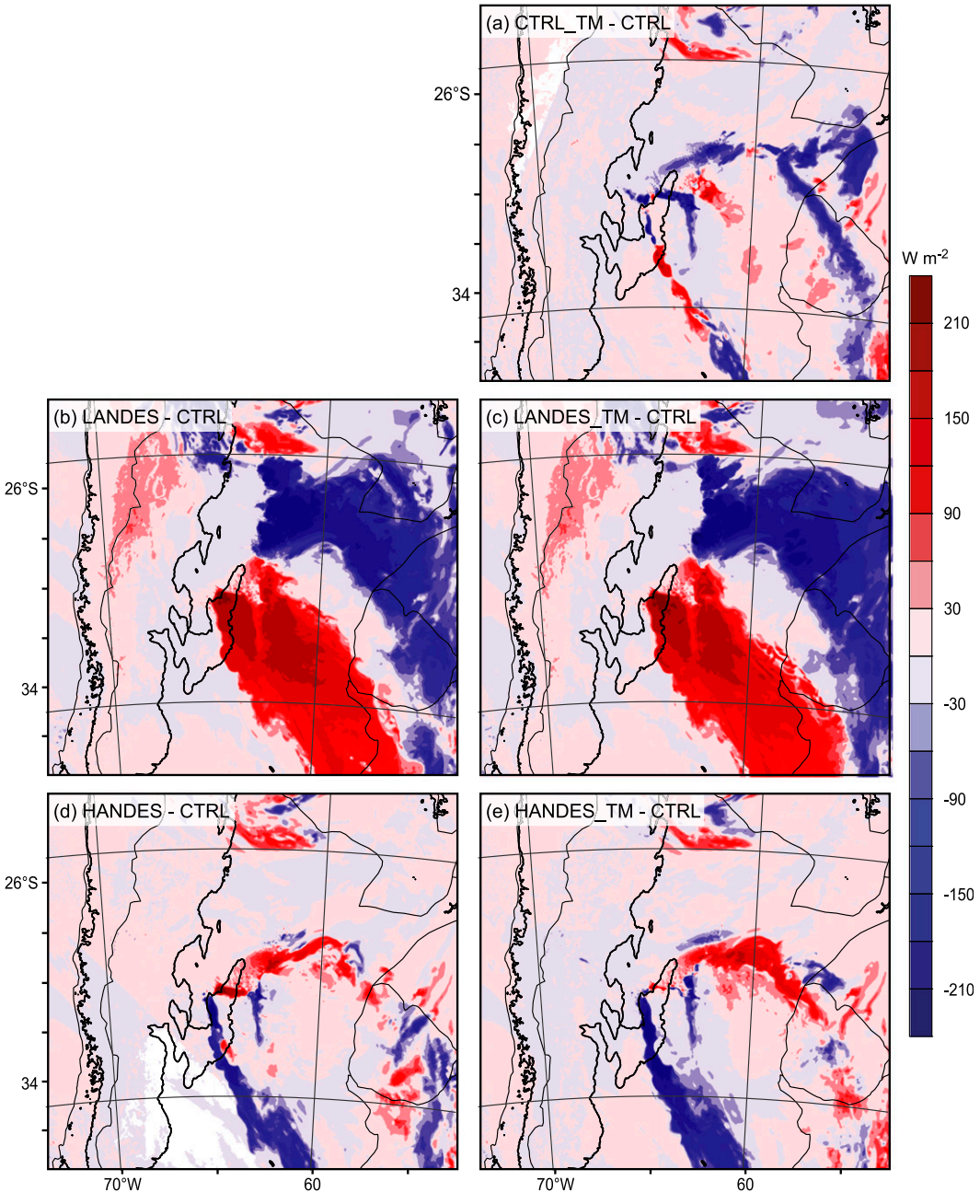

FIG. 11. As in Fig. 10, but at 1000 UTC 27 Dec 2003.

contrast, the CTRL_TM and HANDES_TM simulations without the Sierras de Córdoba produced notably lower echo tops, indicating a decrease in overall convective intensity in the absence of this secondary mountain range. Interestingly, this effect is not observed with the reduced Andes runs (LANDES), suggesting that the different dynamical effects also led to a different mode of convective initiation compared to the full or increased Andes runs. Previous studies have identified that convective initiation by topographic features downstream of other especially high mountain ranges occurs around the world (Medina et al. 2010; Romatschke and Houze 2010). The LANDES runs both showed larger individual instances of 40-dBZ echo tops exceeding 10 km (Fig. 13b), consistent with the larger zone of convective initiation and upscale growth extending much farther east and north compared to the CTRL run (Figs. 10b and 10c). With a lower

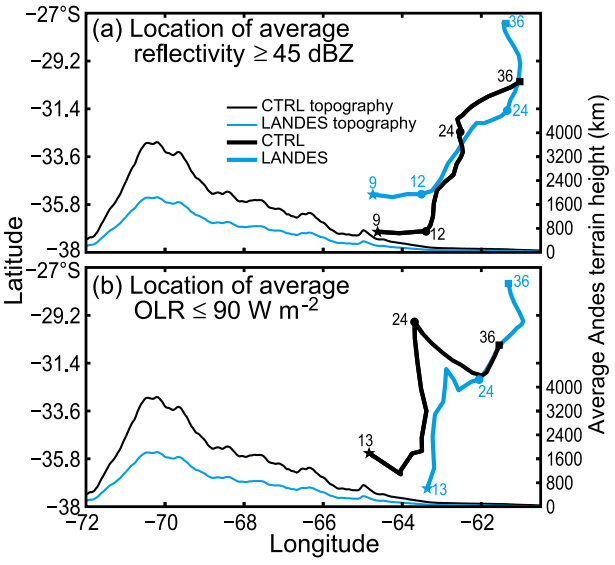

FIG. 12. Storm track of averaged (a) model reflectivity ≥ 45 dBZ and (b) OLR ≤ 90 W m^{-2} in domain 3. In each panel, the terrain modification experiment averages are represented by thick solid lines as shown in the legend. Averaged topography from 25° to 35°S for reference is shown in thin colored lines with the scale axis on the right side of the figure. The symbols represent the following: initial hour (star), intermediate hour (circle), and end hour (square). The small numbers next to each symbol indicate the hour of the simulation, with the following corresponding dates and times: 0900 UTC 26 Dec (9 h), 1200 UTC 26 Dec (12 h), 0000 UTC 27 Dec (24 h), and 1200 UTC 27 Dec (36 h).

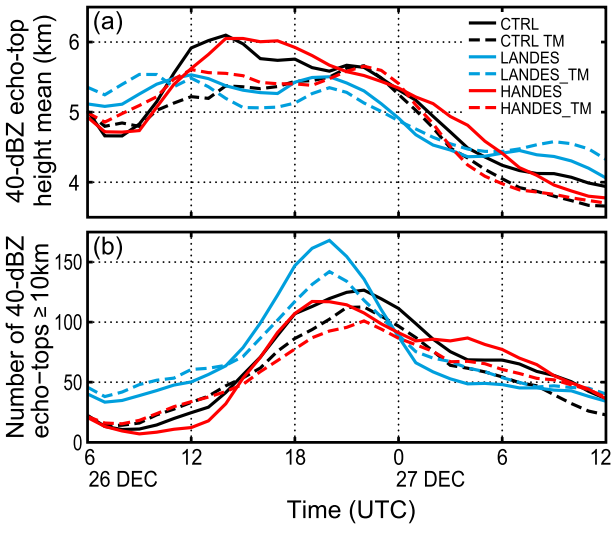

FIG. 13. Echo-top analysis calculated during the entire duration of the WRF simulations for each terrain modification scenario in domain 2 (Fig. 1) showing the (a) 40-dBZ echo-top height mean (km) and (b) number of 40-dBZ echo-tops ≥10 km.

mountain barrier and weaker convective inhibition (shown in section 4h), convection is able to break out at numerous locations instead of the strongly orographically forced and focused convective initiation with the full Andes. Thus, the lower Andes result in more instances of convective initiation, but the storms overall are weaker than the full Andes storms likely because of the differential buildup of convective instability and inhibition.

h. Thermodynamic aspects of terrain modifications

Thermodynamic understanding is crucial to parse the relationship between terrain variations and the resulting convective storms. This section specifically addresses the hypothesis from Rasmussen and Houze (2011) who showed that when storms with WCCs occurred in subtropical South America, lee subsidence related to the mechanical uplift and descent of the midlevel westerlies traversing the Andes Mountains was present in a broad zone between ~20° and 35°S (their Fig. 10). Figure 14 shows two west–east cross sections prior to the first instance of convective initiation in this region (Fig. 14a) and at a later time when developing convection has formed in the lee of the Andes (Fig. 14b). Associated with stronger winds traversing the Andes, midlevel subsiding dry air from ~5 to 10 km overrides the low-level warm moist air mass that prevents instability associated with the warm moist low-level air mass from being released (Fig. 14).

A common way to understand the thermodynamic environment related to convective initiation is to examine the most unstable CAPE and maximum convective inhibition (CIN), which indicate the total amount of potential energy available to the most unstable parcel of air within the lowest 300 hPa of the atmosphere while being lifted to its level of free convection and the amount of energy inhibiting convection, respectively. As mentioned in section 4d, the LANDES run showed more widespread convection in a north–south band downstream of the Andes Mountains (Figs. 10b and 10c), more 40-dBZ echo tops ≥10 km, and lower echo-top height means compared to the higher Andes runs. An example of the difference in maximum convective inhibition in the CTRL and LANDES runs is presented in Fig. 15. A map of the spatial distribution of maximum CIN in the CTRL run (Fig. 15a) shows widespread moderate to strong values of CIN north of the Sierras de Córdoba along the Andes and extending to the east where convection was prevented from occurring in the CTRL run, supporting the orographic connection to the inhibition of convection. In contrast, the lower Andes produce notably weaker CIN downstream of the Andes (Fig. 15b). Lower convective inhibition in the LANDES run implies a higher chance for convection in a widespread region, which is observed in these

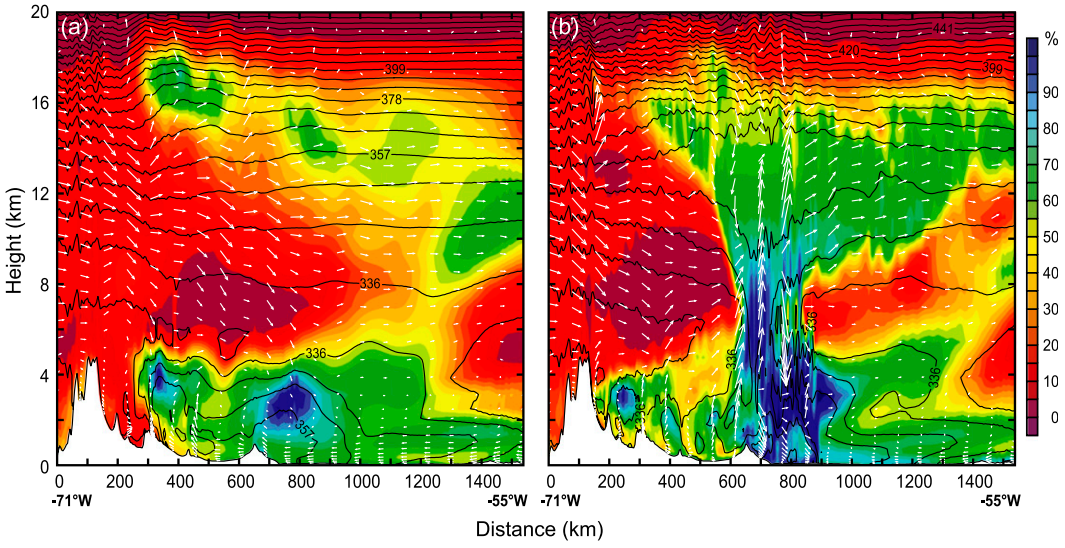

FIG. 14. Vertical cross sections at 30°S with shaded contours of relative humidity (%), black contours of equivalent potential temperature, and white circulation vectors (m s^{-1}) at (a) 1400 UTC 26 Dec 2003 and (b) 2200 UTC 26 Dec 2003. The blue line in Fig. 1 indicates the location of the cross sections. Both panels are from the CTRL simulation in domain 3 with no topography modifications.

simulations. As hypothesized by Rasmussen and Houze (2011), the extreme height of the Andes Mountains and flow up and over the barrier results in significant energy to inhibit convection in the lee (Fig. 15a). Therefore, convective initiation tends to have a strong orographic control in this part of the world as shown in Fig. 15 and supports observational evidence of the narrowly focused region of deep convection in subtropical South America (Zipser et al. 2006; Romatschke and Houze 2010; Rasmussen and Houze 2011; Rasmussen et al. 2014).

Averaged values of CAPE and CIN for each terrain modification experiment were calculated in the SALLJ region (Fig. 1) and their temporal evolution is shown in Fig. 16. In general, the LANDES run has lower values of CAPE throughout the duration of the simulation compared to the CTRL and HANDES runs (between ~200 and 400 J kg^{-1} lower; Fig. 16a). A notable diurnal cycle of CIN, with a nocturnal maximum, is seen in Fig. 16b. During the daytime, solar heating leads to a well-mixed boundary layer that can result in high CAPE and low CIN, while the opposite is true at night (Chaboureau

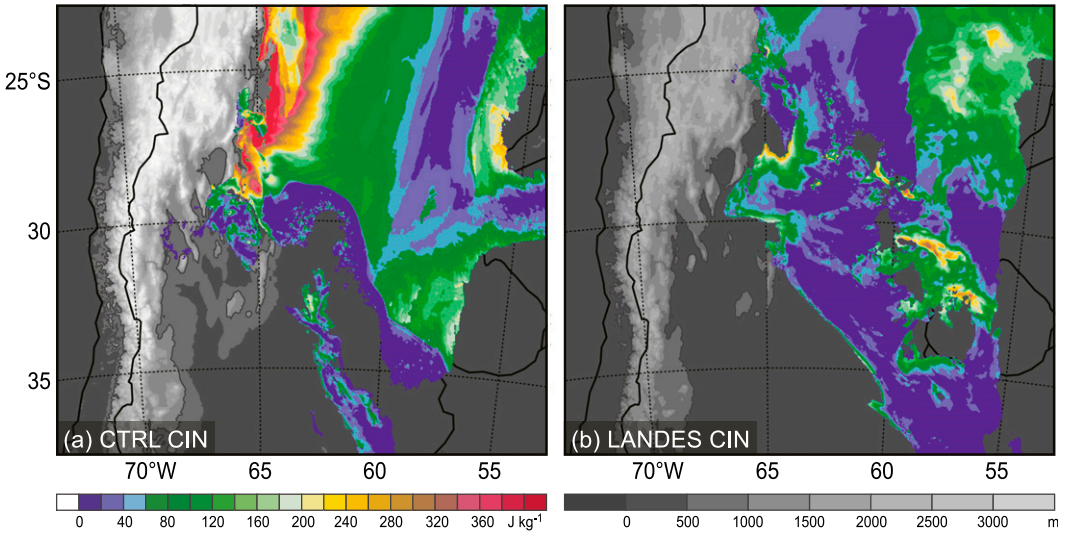

FIG. 15. Comparison of convective inhibition (CIN; J kg^{-1}) in the (a) CTRL and (b) LANDES simulations at 1000 UTC 27 Dec in domain 3.

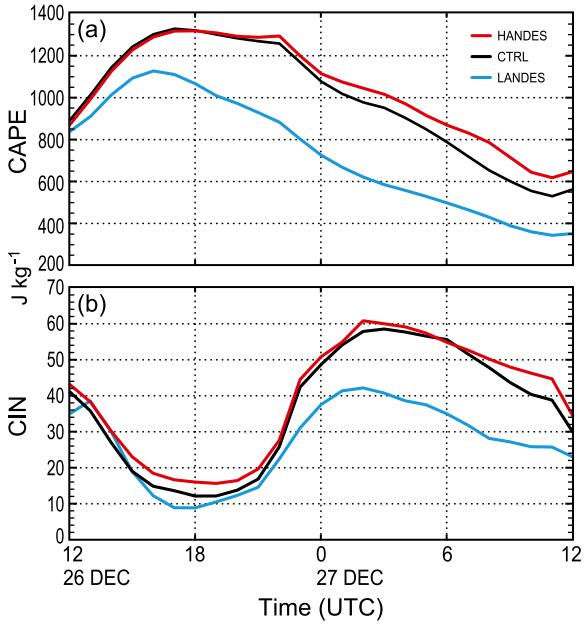

FIG. 16. Time series of (a) convective available potential energy (CAPE) and (b) convective inhibition (CIN) averaged in the SALLJ region from domain 2 (red box in Fig. 1) for the CTRL, LANDES, and HANDES simulations.

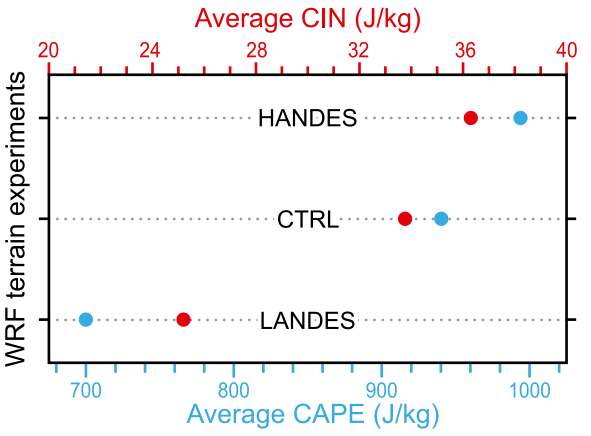

FIG. 17. Summary of the relationship between most unstable CAPE (J kg^{-1}), maximum CIN (J kg^{-1}), and the WRF terrain experiments. Averaged CAPE and CIN values from hours 12–36 of each simulation in the SALLJ region from domain 2 (red box in Fig. 1) are shown in blue and red circles, respectively.

et al. 2004). While the nocturnal maximum of CIN is well documented in observational studies of the United States (e.g., Zhang 2003) and in idealized modeling (e.g., Chaboureau et al. 2004), this particular characteristic has not been previously identified in subtropical South America. From Figs. 15 and 16b, it is evident that the LANDES CIN is generally less than the CTRL and HANDES runs; however, the relative differences between the low and higher Andes runs are most notable between 2000 UTC 26 December and 1200 UTC 27 December. Enhanced nocturnal convective inhibition along the Andes foothills in the presence of relatively high CAPE in the CTRL and HANDES runs likely provides an environment that is conducive to continued nocturnal topographic initiation along the Andes foothills (Fig. 15a). The diurnal cycle of deep convection that persists from the afternoon through the night along the Andes foothills was previously shown using TRMM PR statistics in Rasmussen et al. (2014). Thus, differences in the environment supporting deep convection in subtropical South America and the diurnal cycle magnitude of both CAPE and CIN are modulated by the height of the Andes Mountains.

A more general relationship between the strength of the CAPE and CIN and the height of the mountains is presented in Fig. 17. The higher Andes had greater CAPE and CIN values compared to the reduced Andes values. Lower convective inhibition resulted in more widespread convective initiation and weaker storms (lower CAPE) in the LANDES runs (Figs. 10b,c and 15–17). A taller barrier results in a stronger and deeper SALLJ (Table 5; Campetella and Vera 2002), enhanced integrated moisture flux and MFC (Table 6; Insel et al. 2010), and subsidence in the lee in response to the high mountains. Thus, both CIN and CAPE are expected to increase, making topographic initiation more important since the unstable air has more convective inhibition to overcome.

The current study has investigated the influence of topography on convective initiation near the subtropical Andes. The results from this study are derived from a suite of experiments performed for one particularly intense MCS observed by the TRMM PR. However, this case exhibited properties typified by the TRMM statistics. The generality of the results will need confirmation by future studies. Because of the current sparsity of ground-based data in South America, numerical simulations and detailed thermodynamic analysis will be required in further tests of the conceptual model derived from the present study, discussed in the next section.

5. Conclusions

Numerical simulations of a mesoscale convective system observed by the TRMM PR using various terrain configurations conducted with the NCAR WRF Model extend the satellite observational analysis of convective storms with extreme characteristics in subtropical South America and provide an objective evaluation of storm initiation, development mechanisms, orographic controls, and storm-related bulk thermodynamic characteristics. Sensitivity studies removing and/or reducing

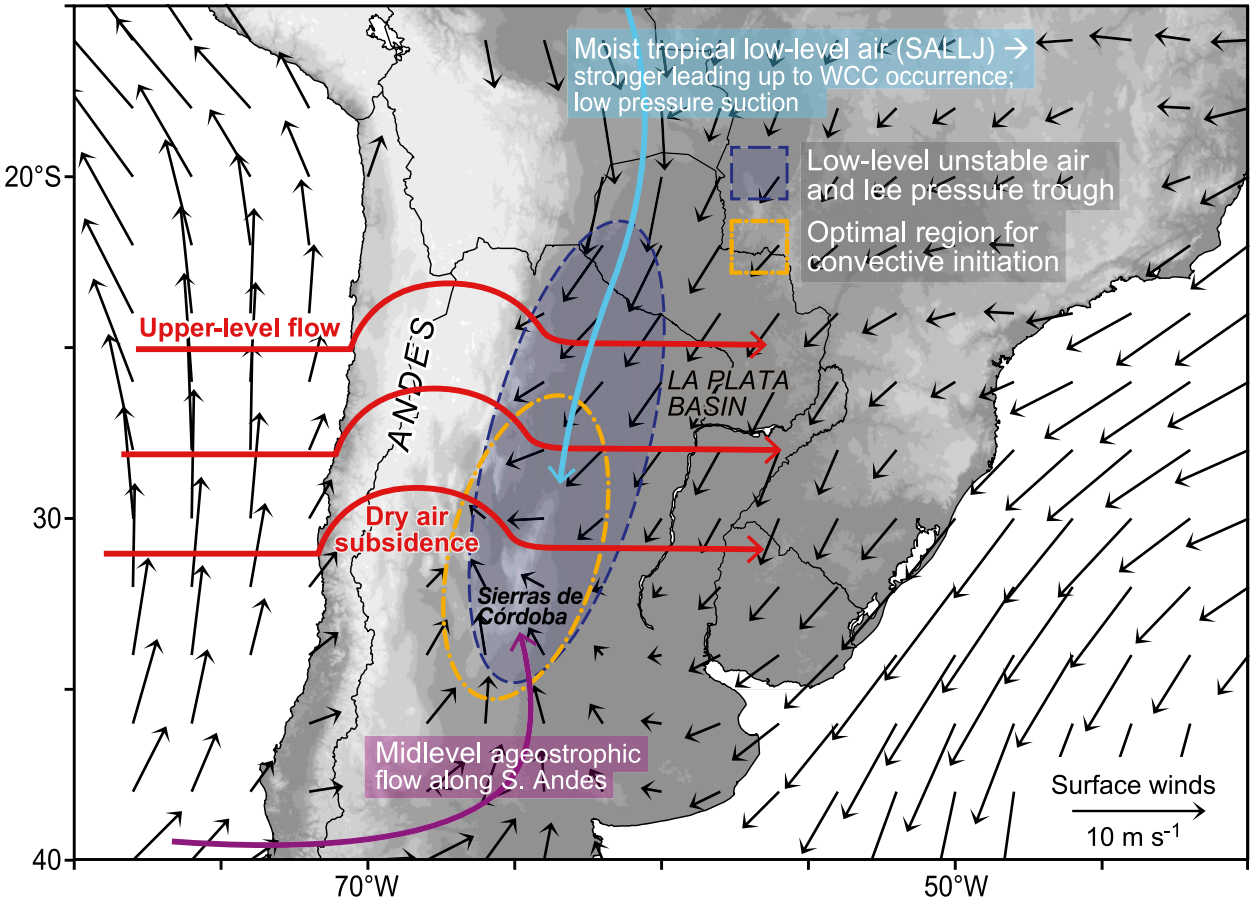

FIG. 18. Conceptual model representing the key ingredients for convective initiation in the lee of the subtropical Andes. Blue arrows and text represent low-level flow, purple arrows and text represent midlevel flow, and red arrows and text represent mid- to upper-level flow. The region highlighted in orange represents the optimal region for convective initiation. Composite surface winds ($m\,s^{-1}$) for days when a wide convective core is located in the La Plata basin regions are represented in black vectors.

various topographic features demonstrate the strong influence of the terrain on the initiation and upscale growth of the subsequent MCSs. The extreme vertical extent of the Andes tends to keep South American MCSs tied to the topography during upscale organization and development related to enhanced lee cyclogenesis and flow modification from a taller mountain range.

A synthesis of the results presented in this study form a conceptual model for convective initiation in subtropical South America (Fig. 18). Enhanced moisture flux of warm and moist low-level air from the Amazon basin via the SALLJ is capped by mid- to upper-level dry air subsidence from the westerlies traversing the Andes Mountains. Leading up to the occurrence of convective storms with extreme characteristics east of the Andes, the strength of the SALLJ, lee cyclone, and moisture fluxes increase in response to synoptic baroclinic waves passing over the southern Andes. Lee cyclogenesis induces a north–south pressure gradient that helps bring air from the SALLJ into the foothills of the Andes instead of its climatological position to the east. Low- to midlevel flow around the southern Andes converges with the SALLJ (Rasmussen and Houze 2011), which is collocated with the Sierras de Córdoba, forming the optimal region for convective initiation in subtropical South America. Thus, while the Sierras de Córdoba help focus and initiate convective storms, they happen to exist in an ideal location to intercept converging air masses from various sources as shown in Fig. 18.

Terrain modification experiments using a mesoscale model provide an objective test of the orographic controls on synoptic-scale disturbances that are related to the occurrence of storms containing WCCs. Results from the modeling experiments provide a greater understanding of the role of the Andes in modulating the synoptic environment leading to convective storms with

extreme characteristics. Lee cyclogenesis downstream of the Andes that was identified in the time-lagged synoptic composites was reproduced in the model simulations. A 50% reduction in the height of the Andes resulted in a weaker lee cyclone magnitude, weaker north–south pressure gradients, and decreased SALLJ strength and moisture flux convergence. In contrast, a 20% increase in the height of the southern Andes strengthened the lee cyclone and the associated north–south pressure gradient force that acted to increase the magnitude of the SALLJ. This increased northerly SALLJ magnitude advected more warm and moist air south to fuel the intense convective storms. Thus, a relationship between the strength of both the lee cyclone and SALLJ, and the height of the Andes is established, showing the profound role of the high mountains in forming the convective storm environment that results in some of the most extreme storms on Earth.

The terrain modification runs led to the following more specific conclusions:

1) A 50% reduction in the Andes resulted in convective initiation being more widespread throughout in a north–south band (extending north to Paraguay) east of the Andes.
2) A mature MCS simulated with the 50% reduced Andes shows that the entire convective system propagated faster to the east, reminiscent of MCSs in the United States.
3) Increasing the southern Andes height increases the flow modification of low-level synoptic disturbances and results in a southward shift of the convective systems.
4) The 50% reduced Andes runs had more echo tops of 40 dB$Z \geq 10$ km than other terrain modification simulations. However, mean 40-dBZ echo-top values for storms simulated with the reduced Andes are weaker overall.
5) Average convective available potential energy and convective inhibition values show that the reduced Andes runs had less convective instability and weaker convective inhibition, while increased Andes runs had both higher CAPE and CIN values.

This study has advanced knowledge and understanding of the role of orography in the initiation and maintenance of storms with extreme characteristics and an improved overall perception of the processes leading to high-impact weather and their simulation near major mountain ranges in subtropical South America. By nature, the study and investigation of high-impact and severe weather has wide-reaching socioeconomic implications. A greater understanding of the formation mechanisms, patterns of development and organization, and severe weather impacts, including hail, flash floods, and tornadoes, resulting from such storms can provide forecasters and the general public with crucial information to save life and property. Argentine storms and MCSs have provided a unique opportunity for the integrated study of high-impact weather and mesoscale modeling, including the orographic control on convective initiation and storm life cycle near the Andes, and the synoptic and mesoscale influence on storm mechanisms. While this study has focused on the Andes, every mountain range and its climatological regime are different, and the way in which convection forms and grows needs to be evaluated in each such orographic situation. As global models become higher in resolution, clouds and precipitation in the vicinities of the world's great mountain ranges will need to be predicted precisely. To guide the development of such models, studies such as this one will need to point out how the fundamental components of synoptic-scale flow, modification of flow by topography, and the creation and release of instability come together to produce the unique convective processes in each major mountainous environment.

Acknowledgments. The authors thank three anonymous reviewers and Daniel Kirschbaum for their comments and suggestions, which have greatly improved this manuscript. Manuel Zuluaga and Megan Chaplin provided helpful comments on this study. Beth Tully coordinated the graphics. This research was sponsored by NSF Grant ATM-0820586, NASA Grants NNX13AG71G and NNX10AH70G, a NASA Earth and Space Science Graduate Fellowship (NNX11AL65H), and a National Center for Atmospheric Research Advanced Study Program (ASP) Postdoctoral Fellowship.

REFERENCES

Altinger de Schwarzkopf, M. L., and L. C. Russo, 1982: Severe storms and tornadoes in Argentina. Preprints, *12th Conf. on Severe Local Storms*, San Antonio, TX, Amer. Meteor. Soc., 59–62.

Banacos, P. C., and D. M. Schultz, 2005: The use of moisture flux convergence in forecasting convective initiation: Historical and operational perspectives. *Wea. Forecasting*, **20**, 351–366, doi:10.1175/WAF858.1.

Buzzi, A., and S. Tibaldi, 1978: Cyclogenesis in the lee of the Alps: A case study. *Quart. J. Roy. Meteor. Soc.*, **104**, 271–287, doi:10.1002/qj.49710444004.

Campetella, C. M., and C. S. Vera, 2002: The influence of the Andes Mountains on the South American low-level flow. *Geophys. Res. Lett.*, **29**, 1826, doi:10.1029/2002GL015451.

Carlson, T. N., S. G. Benjamin, G. S. Forbes, and Y.-F. Li, 1983: Elevated mixed layers in the regional severe storm environment:

Conceptual model and case studies. *Mon. Wea. Rev.*, **111**, 1453–1474, doi:10.1175/1520-0493(1983)111<1453:EMLITR>2.0.CO;2.

Cecil, D. J., 2009: Passive microwave brightness temperatures as proxies for hailstorms. *J. Appl. Meteor. Climatol.*, **48**, 1281–1286, doi:10.1175/2009JAMC2125.1.

——, 2011: Relating passive 37-GHz scattering to radar profiles in strong convection. *J. Appl. Meteor. Climatol.*, **50**, 233–240, doi:10.1175/2010JAMC2506.1.

——, and C. B. Blankenship, 2012: Toward a global climatology of severe hailstorms as estimated by satellite passive microwave imagers. *J. Climate*, **25**, 687–703, doi:10.1175/JCLI-D-11-00130.1.

Chaboureau, J.-P., F. Guichard, J.-L. Redelsperger, and J.-P. Lafore, 2004: The role of stability and moisture in the diurnal cycle of convection over land. *Quart. J. Roy. Meteor. Soc.*, **130**, 3105–3117, doi:10.1256/qj.03.132.

Chen, F., and J. Dudhia, 2001: Coupling an advanced land-surface/hydrology model with the Penn State/NCAR MM5 modeling system. Part I: Model description and implementation. *Mon. Wea. Rev.*, **129**, 569–585, doi:10.1175/1520-0493(2001)129<0569:CAALSH>2.0.CO;2.

Chung, Y. S., 1977: On the orographic influence and lee cyclogenesis in the Andes, the Rockies, and the east Asian mountains. *Arch. Meteor. Geophys. Bioklimatol.*, **26**, 1–12, doi:10.1007/BF02246530.

Davis, C. A., 1997: The modification of baroclinic waves by the Rocky Mountains. *J. Atmos. Sci.*, **54**, 848–868, doi:10.1175/1520-0469(1997)054<0848:TMOBWB>2.0.CO;2.

Douglas, M. W., M. Nicolini, and C. A. Saulo, 1998: Observational evidences of a low level jet east of the Andes during January-March 1998. *Meteorologica*, **23**, 63–72.

Dudhia, J., 1989: Numerical study of convection observed during the winter monsoon experiment using a mesoscale two-dimensional model. *J. Atmos. Sci.*, **46**, 3077–3107, doi:10.1175/1520-0469(1989)046<3077:NSOCOD>2.0.CO;2.

Durkee, J. D., T. L. Mote, and J. M. Shepherd, 2009: The contribution of mesoscale convective complexes into rainfall across subtropical South America. *J. Climate*, **22**, 4590–4605, doi:10.1175/2009JCLI2858.1.

Emanuel, K. A., M. Fantini, and A. J. Thorpe, 1987: Baroclinic instability in an environment of small stability to slantwise moist convection. Part I: Two-dimensional models. *J. Atmos. Sci.*, **44**, 1559–1573, doi:10.1175/1520-0469(1987)044<1559:BIIAEO>2.0.CO;2.

Gan, M. A., and V. B. Rao, 1994: The influence of the Andes Cordillera on transient disturbances. *Mon. Wea. Rev.*, **122**, 1141–1157, doi:10.1175/1520-0493(1994)122<1141:TIOTAC>2.0.CO;2.

Gutzler, D. S., and T. M. Wood, 1990: Structure of large-scale convective anomalies over tropical oceans. *J. Climate*, **3**, 483–496, doi:10.1175/1520-0442(1990)003<0483:SOLSCA>2.0.CO;2.

Hong, S.-Y., Y. Noh, and J. Dudhia, 2006: A new vertical diffusion package with an explicit treatment of entrainment processes. *Mon. Wea. Rev.*, **134**, 2318–2341, doi:10.1175/MWR3199.1.

Houze, R. A., Jr., 2004: Mesoscale convective systems. *Rev. Geophys.*, **42**, RG4003, doi:10.1029/2004RG000150.

——, 2014: *Cloud Dynamics*. 2nd ed. Academic Press/Elsevier, 432 pp.

——, B. F. Smull, and P. Dodge, 1990: Mesoscale organization of springtime rainstorms in Oklahoma. *Mon. Wea. Rev.*, **118**, 613–654, doi:10.1175/1520-0493(1990)118<0613:MOOSRI>2.0.CO;2.

——, D. C. Wilton, and B. F. Smull, 2007: Monsoon convection in the Himalayan region as seen by the TRMM Precipitation Radar. *Quart. J. Roy. Meteor. Soc.*, **133**, 1389–1411, doi:10.1002/qj.106.

——, K. L. Rasmussen, S. Medina, S. R. Brodzik, and U. Romatschke, 2011: Anomalous atmospheric events leading to the summer 2010 floods in Pakistan. *Bull. Amer. Meteor. Soc.*, **92**, 291–298, doi:10.1175/2010BAMS3173.1.

——, ——, M. D. Zuluaga, and S. R. Brodzik, 2015: The variable nature of convection in the tropics and subtropics: A legacy of 16 years of the Tropical Rainfall Measuring Mission satellite. *Rev. Geophys.*, **53**, 994–1021, doi:10.1002/2015RG000488.

Iguchi, T., T. Kozu, R. Meneghini, J. Awaka, and K. Okamoto, 2000: Rain-profiling algorithm for the TRMM precipitation radar. *J. Appl. Meteor.*, **39**, 2038–2052, doi:10.1175/1520-0450(2001)040<2038:RPAFTT>2.0.CO;2.

——, ——, J. Kwiatkowski, R. Meneghini, J. Awaka, and K. Okamoto, 2009: Uncertainties in the rain profiling algorithm for the TRMM precipitation radar. *J. Meteor. Soc. Japan*, **87A**, 1–30, doi:10.2151/jmsj.87A.1.

Insel, N., C. J. Poulsen, and T. A. Ehlers, 2010: Influence of the Andes Mountains on South American moisture transport, convection, and precipitation. *Climate Dyn.*, **35**, 1477–1492, doi:10.1007/s00382-009-0637-1.

Kain, J. S., and J. M. Fritsch, 1993: Convective parameterization for mesoscale models: The Kain-Fritsch scheme. *The Representation of Cumulus Convection in Numerical Models, Meteor. Monogr.*, No. 46, Amer. Meteor. Soc., 165–170.

Kalnay, E., and Coauthors, 1996: The NCEP/NCAR 40-Year Reanalysis Project. *Bull. Amer. Meteor. Soc.*, **77**, 437–471, doi:10.1175/1520-0477(1996)077<0437:TNYRP>2.0.CO;2.

Kasahara, A., 1966: The dynamical influence of orography on the large-scale motion of the atmosphere. *J. Atmos. Sci.*, **23**, 259–271, doi:10.1175/1520-0469(1966)023<0259:TDIOOO>2.0.CO;2.

Marengo, J., W. Soares, C. Saulo, and M. Nicolini, 2004: Climatology of the LLJ east of the Andes as derived from the NCEP reanalyses. *J. Climate*, **17**, 2261–2280, doi:10.1175/1520-0442(2004)017<2261:COTLJE>2.0.CO;2.

Matsudo, C. M., and P. V. Salio, 2011: Severe weather reports and proximity to deep convection over Northern Argentina. *Atmos. Res.*, **100**, 523–537, doi:10.1016/j.atmosres.2010.11.004.

McGinley, J. A., 1982: A diagnosis of Alpine lee cyclogenesis. *Mon. Wea. Rev.*, **110**, 1271–1287, doi:10.1175/1520-0493(1982)110<1271:ADOALC>2.0.CO;2.

Medina, S., R. A. Houze Jr., A. Kumar, and D. Niyogi, 2010: Summer monsoon convection in the Himalayan region: Terrain and land cover effects. *Quart. J. Roy. Meteor. Soc.*, **136**, 593–616, doi:10.1002/qj.601.

Mlawer, E. J., S. J. Taubnam, P. D. Brown, M. J. Iacono, and S. A. Clough, 1997: Radiative transfer for inhomogeneous atmospheres: RRTM, a validated correlated-k model for the longwave. *J. Geophys. Res.*, **102**, 16 663–16 682, doi:10.1029/97JD00237.

Nascimento, E. L., and I. P. V. O. Marcelino, 2005: Preliminary analysis of the 3 January 2005 tornadoes in Criciuma/SC. *Bull. Braz. Meteor. Soc.*, **29**, 33–44.

Nogués-Paegle, J., and K. C. Mo, 1997: Alternating wet and dry conditions over South America during summer. *Mon. Wea. Rev.*, **125**, 279–291, doi:10.1175/1520-0493(1997)125<0279:AWADCO>2.0.CO;2.

Palmén, E., and C. W. Newton, 1969: *Atmospheric Circulation Systems*. Academic Press, 603 pp.

Rasmussen, K. L., 2014: On the nature of severe orographic thunderstorms near the Andes in subtropical South America. Ph.D. dissertation, University of Washington, 227 pp.

——, and R. A. Houze Jr., 2011: Orogenic convection in subtropical South America as seen by the TRMM satellite. *Mon. Wea. Rev.*, **139**, 2399–2420, doi:10.1175/MWR-D-10-05006.1.

——, S. L. Choi, M. D. Zuluaga, and R. A. Houze Jr., 2013: TRMM precipitation bias in extreme storms in South America. *Geophys. Res. Lett.*, **40**, 3457–3461, doi:10.1002/grl.50651.

——, M. D. Zuluaga, and R. A. Houze Jr., 2014: Severe convection and lightning in subtropical South America. *Geophys. Res. Lett.*, **41**, 7359–7366, doi:10.1002/2014GL061767.

——, A. J. Hill, V. E. Toma, M. D. Zuluaga, P. J. Webster, and R. A. Houze Jr., 2015: Multiscale analysis of three consecutive years of anomalous flooding in Pakistan. *Quart. J. Roy. Meteor. Soc.*, **141**, 1259–1276, doi:10.1002/qj.2433.

——, M. M. Chaplin, M. D. Zuluaga, and R. A. Houze Jr., 2016: Contribution of extreme convective storms to rainfall in South America. *J. Hydrometeor.*, **17**, 353–367, doi:10.1175/JHM-D-15-0067.1.

Romatschke, U., and R. A. Houze, 2010: Extreme summer convection in South America. *J. Climate*, **23**, 3761–3791, doi:10.1175/2010JCLI3465.1.

Rozante, J. R., and I. F. A. Cavalcanti, 2008: Regional Eta model experiments: SALLJEX and MCS development. *J. Geophys. Res.*, **113**, D17106, doi:10.1029/2007JD009566.

Salio, P., M. Nicolini, and E. J. Zipser, 2007: Mesoscale convective systems over southeastern South America and their relationship with the South American low-level jet. *Mon. Wea. Rev.*, **135**, 1290–1309, doi:10.1175/MWR3305.1.

Satyamurty, P., C. C. Ferreira, and M. A. Gan, 1990: Cyclonic vortices over South America. *Tellus*, **42A**, 194–201, doi:10.1034/j.1600-0870.1990.00016.x.

Saulo, A. C., M. Nicolini, and S. C. Chou, 2000: Model characterization of the South American low-level flow during the 1997–1998 spring-summer season. *Climate Dyn.*, **16**, 867–881, doi:10.1007/s003820000085.

Schultz, D. M., and C. A. Doswell III, 2000: Analyzing and forecasting Rocky Mountain lee cyclogenesis often associated with strong winds. *Wea. Forecasting*, **15**, 152–173, doi:10.1175/1520-0434(2000)015<0152:AAFRML>2.0.CO;2.

Skamarock, W. C., and Coauthors, 2008: A description of the Advanced Research WRF version 3. NCAR Tech. Note NCAR/TN-475+STR, 113 pp., doi:10.5065/D68S4MVH.

Smith, R. B., 1984: A theory of lee cyclogenesis. *J. Atmos. Sci.*, **41**, 1159–1168, doi:10.1175/1520-0469(1984)041<1159:ATOLC>2.0.CO;2.

——, 1986: Further development of a theory of lee cyclogenesis. *J. Atmos. Sci.*, **43**, 1582–1602, doi:10.1175/1520-0469(1986)043<1582:FDOATO>2.0.CO;2.

Thompson, G., P. R. Field, R. M. Rasmussen, and W. D. Hall, 2008: Explicit forecasts of winter precipitation using an improved bulk microphysics scheme. Part II: Implementation of a new snow parameterization. *Mon. Wea. Rev.*, **136**, 5095–5115, doi:10.1175/2008MWR2387.1.

Velasco, I., and J. M. Fritsch, 1987: Mesoscale convective complexes in the Americas. *J. Geophys. Res.*, **92**, 9591–9613, doi:10.1029/JD092iD08p09591.

Vera, C., and Coauthors, 2006: The South American Low-Level Jet Experiment. *Bull. Amer. Meteor. Soc.*, **87**, 63–77, doi:10.1175/BAMS-87-1-63.

Yuan, J., and R. A. Houze Jr., 2010: Global variability of mesoscale convective system anvil structure from A-train satellite data. *J. Climate*, **23**, 5864–5888, doi:10.1175/2010JCLI3671.1.

Zhang, G. J., 2003: Roles of tropospheric and boundary layer forcing in the diurnal cycle of convection in the U.S. southern great plains. *Geophys. Res. Lett.*, **30**, 2281, doi:10.1029/2003GL018554.

Zipser, E. J., D. J. Cecil, C. Liu, S. W. Nesbitt, and D. P. Yorty, 2006: Where are the most intense thunderstorms on Earth? *Bull. Amer. Meteor. Soc.*, **87**, 1057–1071, doi:10.1175/BAMS-87-8-1057.

Zuluaga, M. D., and R. A. Houze Jr., 2013: Evolution of the population of precipitating convective systems over the equatorial Indian Ocean in active phases of the Madden–Julian oscillation. *J. Atmos. Sci.*, **70**, 2713–2725, doi:10.1175/JAS-D-12-0311.1.

——, and ——, 2015: Extreme convection of the near-equatorial Americas, Africa, and adjoining oceans as seen by TRMM. *Mon. Wea. Rev.*, **143**, 298–316, doi:10.1175/MWR-D-14-00109.1.